Energy-efficient indirect evaporative cooler design framework: An experimental and numerical study

Muhammad Ahmad Jamil[a,*,**], Muhammad Wakil Shahzad[a,**,*], Ben Bin Xu[a], Muhammad Imran[b], Kim Choon Ng[c], Syed M. Zubair[d], Christos N. Markides[e], William M. Worek[f]

[a] Mechanical & Construction Engineering Department, Northumbria University, Newcastle Upon Tyne, UK.
[b] Department of Mechanical, Biomedical and Design Engineering, Aston University, Birmingham B4 7ET, UK
[c] Water Desalination and Reuse Center, King Abdullah University of Science and Technology, Thuwal, Saudi Arabia.
[d] Mechanical Engineering Department, King Fahd University of Petroleum & Minerals, Dhahran, Saudi Arabia.
[e] Clean Energy Processes (CEP) Laboratory, Department of Chemical Engineering, Imperial College London, London SW7 2AZ, UK.
[f] Building and Industrial Technologies Energy Systems and Infrastructure Analysis Division, Argonne National Laboratory, Lemont, IL 60439, United States

Corresponding Authors, email: *muhammad2.ahmad@northumbria.ac.uk ,
**muhammad.w.shahzad@northumbria.ac.uk

** *The two authors have the same contribution to this study*

ABSTRACT

A remarkable surge in cooling demand is observed in the last decades. Currently, the cooling market is dominated by mechanical vapor compression chillers which are energy intensive and use harmful chemical refrigerants. Therefore, the current focus of the current research in cooling is the development of unconventional, sustainable cooling systems. In this regard, indirect evaporative coolers have shown significant potential (particularly under hot-dry climates) with high energy efficiency, low cost, water-based sustainable operation, and benign emissions. However, these systems are in the development stage and have not yet been fully commercialized because of certain design challenges. An innovative indirect evaporative cooler is proposed, fabricated, and experimentally tested in this study. Particularly, the study is focused on the development of heat transfer coefficient correlation for the system for commercial-scale design and expansion. This is because the earlier available correlation is based on simple airflow between parallel plates assumption and does not incorporate the effect of the evaporative potential of the system resulting in under/over-estimation of the heat transfer characteristics. The results showed that the proposed system achieved a temperature drop of 20 °C, a cooling capacity of around 180 W, and an overall heat transfer coefficient of up to 30 W/m^{2}K. Moreover, the study presents an experiment-regression-based heat transfer coefficient correlation that satisfactorily captures the effect of outdoor air temperature and airflow rate ratio which are critical in the design of evaporative coolers. The proposed correlation showed a high (±5%) with experimental data thus making it suitable for the future design of IEC systems over assorted operating scenarios.

Keywords: novel indirect evaporative cooler, heat transfer coefficient correlation, sustainable cooling, experiments

1. Introduction

Comfort cooling is now perceived as a social imperative and is believed to improve the working efficiency of humans and technology [1]. Therefore, its demand is increasing exponentially due to various drivers including the warming planet, population growth, urbanization, and high-income growth (refer to Figure 1) [2]. The cumulative impact of these drivers is triggering the air conditioning demand. So based on the business-as-usual scenario of 2018, the global air conditioners (ACs) are predicted to ramp up to 5.6 billion in 2050 with room ACs (mini split+ packaged) alone exceeding 4.5 billion [2]. It implies that around 10 AC units will be sold every second in the next 30 years and particularly the developing regions will face a fivefold increased demand for room air conditioners [3]. The more serious concerns with piling AC units are energy consumption and emissions [4,5]. A threefold increase in global AC-related energy is expected by 2050, aggregating the total demand to 7700 terawatt-hours (TWh) from 2300 TWh in 2017 [6,7]. Similarly, AC CO_2 emissions have tripled to 1600 million metric tons since 1990 [8] and are expected to cross 167 gigatons of CO_2 equivalent by 2050 [9]. The cooling market is captured by vapor compression technology which is responsible for high energy consumption and emissions [10,11]. So a water-based cooling solution is required to minimize energy consumption and emissions.

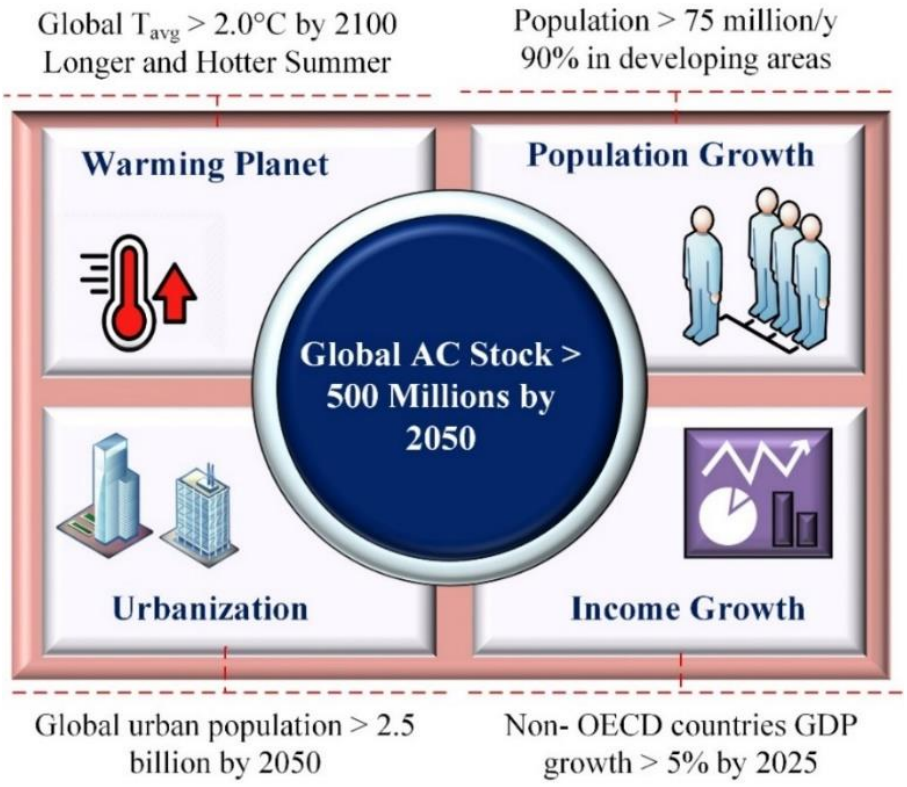

Figure 1. Drivers for fast-rising cooling demand [2].

Evaporative cooling has emerged as the only viable solution because of significantly low energy consumption, water-based operation, and benign emissions [12,13]. However, the conventional direct evaporative coolers (using Aspen, Khus fibers cellulose paper sheets, etc.) have limited applications due to high humidity (100%) issues in the supply air [14–16]. While an advanced idea of indirect evaporative cooling (IEC) resolves the issue of high humidity and has the potential to outperform conventional vapor compression systems sustainably [17]. It uses water as a refrigerant and evaporative potential of air and provides humidity-controlled cooling [18,19]. These systems handle latent and sensible cooling loads separately thus offering individual process optimization without any rigid operational limitations [20]. Therefore, these can achieve a COP ranging from >30 (for only cooling) and 10-12 for overall systems (including the dehumidification process) [21]. Therefore, these systems can be employed for various applications [22,23] like human comfort [24], artifacts preservation [25], animal comfort [26], agricultural product storage [27], and energy recovery for vapor compression systems [28–30]. Above all, the current carbon neutrality demand is favoring sustainable solutions as recommended by Dai et al. [31]. Keeping in view the extensive applications and advantages, significant research is conducted to investigate and improve IEC system performance [32–34]. However, the commercial-scale deployment of these systems is subject to addressing certain design limitations [35]. These include heat transfer improvement, effective water management, operational reliability, and heat transfer wall development [36]. This is because, in the typical IEC systems, these issues have been reported to be the major design challenges for commercial scale realization. Particularly, the water showering inside the heat exchanger complicates the wall development with multi-layers, lowers heat transfer, increases maintenance issues, and obstructs water management.

The current study investigates a novel IEC system that addresses the design challenges in conventional IEC systems through the rearrangement and retrofitting of new components in the system. Particularly, the study is focused on the development of heat transfer coefficient correlation for the proposed system for accurate heat transfer modeling of the system. This is because the earlier studies on IEC use typical heat exchanger correlations for the calculation of heat transfer coefficients in dry and wet channels. These are based on the concept of airflow between parallel plates and the effect of evaporation and outdoor air temperature variations is not properly captured in these calculations. Therefore, these correlations under/over-estimate the heat transfer area requirement misleading the cooling capacity which is critical for large-scale systems. A robust experimental-based heat transfer coefficient correlation development is conducted for the IEC systems which was missing earlier. For this purpose, a critical review

of existing heat transfer correlations is conducted first. It comprehensively summarized the mathematical formulation, operational conditions, assumptions, applicability ranges, reported values, and characteristics under different operational conditions. This is followed by the design and development of an experimental test rig based on the proposed operational configuration. Then a detailed experimental investigation of the system performance under assorted outdoor air temperature and working air flow rate conditions. The experimental data is then used to calculate the overall heat transfer coefficient. Then the theoretical model is applied to estimate the local dry and wet channel heat transfer coefficients. Finally, the experimental data is used to formulate heat transfer coefficient correlation using regression. The proposed correlations showed good agreement (±5%) with the experimental data and can be used for commercial scale design of IEC systems.

2. Heat transfer correlations for indirect evaporative coolers

2.1. Flat plates

One of the important and frequently adopted formulae was developed by Ranz and Marshall [37] in 1952 (C-1). They proposed a model to calculate the heat transfer from water droplets due to evaporation in terms of Reynolds number, and Prandtl number with constants as given below. It has been used extensively used in recent studies [38–44].

$$Nu = 2 + 0.6\,\mathrm{Re}^{0.5}\,\mathrm{Pr}^{0.33} \tag{1}$$

Lin et al. [45] developed correlations for the calculation of Nu for dry and wet channels and also Sherwood number (Sh) by studying the heat and mass transfer process for a dewpoint indirect evaporative cooler. They reported the average convection heat and mass transfer coefficients as 26.8 to 29.9 W/m^2·K, and 0.025 to 0.027 m/s, and the Nu for the dry and wet side as 8.67 to 9.95, 8.68 to 9.21 and 8.17 to 8.67.

$$Nu_{WA} = 1.605\,\mathrm{Re}_D^{0.0117}\left(h_{fg}\,D_{va}\,\Delta\rho_{v,sa}/k_f\,\Delta T_{dp}\right)^{0.1438} \left(-0.800AFR^3 + 2.0249AFR^2 - 0.9085AFR + 7.5\right) \tag{2}$$

$$Sh_{WA} = 16.625\,\mathrm{Re}_D^{0.018}\,\pi^{0.2901} \tag{3}$$

Wan et al. [46] developed heat and mass transfer correlations for IEC with condensation in the dry channel. The study used the orthogonal test method and experimentally validated the CFD model based on COMSOL as given below

$$h_{OA} = 134.684\,T_{OA,i}^{0.014}\,RH_{OA,i}^{0.023}\,V_{OA,i}^{0.013}\,L^{-0.048}\,b_{ch}^{-1.001} \tag{4}$$

$$h_{m,OA} = 498.132 T_{OA,i}^{-0.727} RH_{OA,i}^{-0.950} V_{OA,i}^{0.112} T_{OA,i}^{0.442} RH_{OA,i}^{0.164} b_{ch}^{-0.800} \quad (5)$$

$$h_{WA} = 85.155 T_{OA,i}^{-0.164} RH_{OA,i}^{-0.141} T_{WA,i}^{0.327} b_{ch}^{-1.176} \quad (6)$$

$$h_{m,WA} = 132.139 T_{OA,i}^{0.127} RH_{WA,i}^{0.140} b_{ch}^{-1.243} \quad (7)$$

Another correlation was developed by Dowdy and Karabash [47] for direct evaporative coolers with the surface covered by a rigid cellulose media saturated with water. The correlation is modified in terms of *Re, Pr*, characteristics length, and evaporation surface thickness and is used for IEC applications [22,47–52].

$$Nu = 0.1\left(le/l\right)^{0.12} \mathrm{Re}^{0.8} \mathrm{Pr}^{0.33} \quad (8)$$

In addition to the above-mentioned formulations, some standard correlations have also been used for the heat transfer study of IEC systems. A summary of these correlations is presented in Table 1.

Table 1.
Standard heat transfer correlations are used for IEC systems.

Sr#	Correlation	Ref
1.	$Nu_{OA} = 6.7932 \mathrm{Re}_D^{0.0324} r^{-0.016}$	[45]
2.	$Nu = 0.023 \mathrm{Re}^{0.8} \mathrm{Pr}^{0.33}$ Used for both dry air, wet air as well as water to calculate heat transfer coefficient. For wet channels, an accompanying mass transfer is also calculated. For thermally fully developed turbulent flows region (Dittus–Boelter correlation).	[35,39,40,53–57]
3.	$Nu = 8.235 + 0.0364 \mathrm{Re}\,\mathrm{Pr}\left(D_h/L\right)$ Mostly used for dry channel and standard correlation for a parallel passage with uniform heat flux	[58]
4.	$Nu = \left[\left(1.49 \cdot y^{*-1/3}\right)^{4.5} + 8.235^{4.5}\right]^{1/4.5}$ $y^* : y/D_h \,\mathrm{Re}\,\mathrm{Pr}$ Mostly applied for the dry channel side of IEC and initially proposed by Awad [48] for high-width-to-height rectangular channels	[42] [47–50] [48]
5.	$Nu = 7.4 + \frac{0.03\left(D_h/L_{plate}\right)\mathrm{Re}\,\mathrm{Pr}}{1 + 0.016\left[\left(D_h/L_{plate}\right)\mathrm{Re}\,\mathrm{Pr}\right]^{(2/3)}}$ The flow between isothermal parallel plates	[59]
6.	$Nu = 8.235\begin{pmatrix}1 - 2.042\left(b/e\right) + 3.085\left(b/e\right)^2 - 2.447\left(b/e\right)^3 \\ +1.058\left(b/e\right)^4 - 0.186\left(b/e\right)^5\end{pmatrix}$	[22,51]

	Where b/e = aspect ratio Used for dry channel only and standard rectangular dry channel with constant surface flux.	
7.	$Nu = 7.541(1-2.610(b/e)+4.970(b/e)^2$ $-5.119(b/e)^3+2.702(b/e)^4-0.548(b/e)^5)$ Where b/e = 0.066 is the aspect ratio (minimum/maximum) For a laminar, hydrodynamically, and thermally fully developed flow in a rectangular duct that is exposed to a uniform wall temperature	[59]
8.	$Nu = 1.86\left(Re_{D_h} Pr\left(D_h/L\right)\right)^{1/3}\left(\mu/\mu_w\right)^{0.14}$ Used for both dry and wet channels for Nu including the thermal entrance region as well as in the thermally developed region	[58] [60–66]
9.	$Nu = 0.332\,\mathrm{Re}^{0.5}.\mathrm{Pr}^{0.33}(\mathrm{Re}<5\times10^4)$ Laminar $Nu = 0.0292\,\mathrm{Re}^{0.8}\,\mathrm{Pr}^{0.33}(5\times10^4\,\mathrm{Re}<3\times10^7)$ Turbulent $Nu = 0.664R\mathrm{e}^{1/2}\,\mathrm{Pr}^{0.333}$ Flow over a flat plate	[67][68] [69,70]
10.	$Nu = 3.66+\dfrac{0.0668\,\mathrm{Re}\,\mathrm{Pr}\,D_h/L_{plate}}{1+0.04\left[D_h/L_{plate}\,\mathrm{Re}\,\mathrm{Pr}\right]^{(2/3)}}$ Used for the dry channel, For thermal entrance region, and for average Nusselt number	[60,69,71]

2.2. Enhanced surfaces

Besides plain surface geometry, enhanced surfaces with patterns, fins, and protrusions have also been used in IECs for higher heat transfer rates. Therefore, formulations have also been developed to estimate the heat transfer characteristics of these surfaces. For instance, Antonellis et al. [72] developed the heat transfer correlation (for Aluminum alloy plates with surface dimples based on the concepts of enhanced surface heat transfer [73,74]. They showed that the most influential parameters affecting heat transfer include dimples height, pitch, size, and placement. They developed the correlation in terms of Re and Pr with constants. Where the values for constants were calculated by minimizing the error in dry bulb effectiveness and the results obtained from simulation and experiments. A summary of these correlations is presented in Table 2.

Table 2.
Heat transfer coefficient correlations for enhanced surface heat transfer for IEC systems.

Sr #	Correlation	Ref
1.	**IEC with a dimpled surface** $h = \left(k/D_h\right)\alpha R\mathrm{e}^{\beta}\,\mathrm{Pr}^{0.333}\left(700<\mathrm{Re}<2300\right)$ $\alpha = 0.0185, \beta = 0.928$ For dry and wet channels with dimples on the plate	[69,75,76]

2.	**IEC with enhanced plate patterns** $$Nu_{capsule} = 0.65\,\mathrm{Re}^{0.581}\,\mathrm{Pr}^{0.317}$$ $$Nu_{fin} = 0.59\,\mathrm{Re}^{0.457}\,\mathrm{Pr}^{0.333}$$ $$Nu_{corrugated} = \left(8.235^3 + Nu_t^3\right)^{1/3}$$ $$Nu_t = \left\{0.0205 + 1.15\left(p_p/p_c\right)^{1.18}\right\}\mathrm{Re}^{0.8-0.2\left(p_p/p_c\right)}$$ For dry channel side with enhanced plate patterns	[38,77–79]
3.	**IEC With internal baffles in the dry channel side** $$Nu = 0.103\,\mathrm{Re}^{0.759}\,\mathrm{Pr}^{0.4}\left(L/s_d\right)^{0.167}\left(S_h/S_p\right)$$ S_d distance between baffle (m) S_h baffle height (m) S_p the gap between the plate (m) Used only for dry channels with internal baffles	[69,80,81]

2.3. Ranges and characteristics of earlier IEC heat transfer coefficients

The above heat transfer review shows that a variety of correlations for Nusselt number/heat transfer coefficient are reported for different operating scenarios. However, the actual quantitative values for Nu/h are seldom reported because most of the earlier studies report IEC performance in terms of cooling capacity, coefficient of performance, or efficiencies. However, the heat transfer coefficients are of paramount significance for IEC as these govern the heat transfer process and control the area footprints and economics of the system. A higher heat transfer coefficient results in a lower heat transfer area and reduced capital cost requirements. A comprehensive summary of the reported values for Nusselt number, local, and overall heat transfer coefficients alongside the geometric and process parameters are presented in Table 3. It shows that in most of the studies, the heat transfer coefficient is calculated using constant surface temperature or constant surface heat flux approach-based correlations. Therefore, the value for Nu varies between 7-8 for constant heat flux and 4-5 for constant surface temperature cases thus calculating the heat transfer coefficient 20-30 W/m^{2}K. However, it is also important to mention that the heat transfer coefficient values increase considerably under special working conditions of systems. For instance, under condensation in the dry channel conditions, the heat transfer coefficient is reported to vary between 180-200 W/m^{2}K. Similarly, under direct-indirect hybrid system operation conditions, the overall heat transfer coefficient is reported to vary between 100-400 W/m^{2}K. Likewise, the heat transfer coefficient for porous ceramic tubular-based IEC system is reported up to 80 W/m^{2}K.

Table 3.
Heat transfer coefficient correlations for enhanced surface heat transfer for IEC systems.

Study description	**Geometry** L×W×H (mm)	**Flow parameter**	**Reported values**	**Ref.**
Counterflow Exp + Sim	800×180×4	V_{OA} = 2 m/s AFR = 33%	Nu: 8.67-9.95 h: 25-30	[45]
Counterflow Sim	1250×NA×5	V_{OA} = 2.75 m/s AFR = 100%	h: 20.5	[46]
Crossflow & Counterflow Sim	1100×325×6	m_{OA} = 2000 m^3/h AFR = 50%	Nu: 8.235*	[58]
Counterflow Exp + Sim	1200×80×5	V_{OA} = 2.4 m/s AFR = 33%	Nu: 8.235*	[82]
Counterflow Exp	210×120×4	m_{OA} = 0.03 kg/s m_{OA} = 0.012 kg/s	h: 8.26-13.06 U: 6.90	[70]
Crossflow (Condensation on the dry side) Exp+sim	400×250×0.4	V_{OA} = 2.5 m/s AFR = 100%	h: 180-250	[83]
Counterflow Sim	500×500×3.5	m_{OA} = 0.0014 kg/s m_{WA} = 0.00098 kg/s AFR = 70%	Nu: 4.861**	[84]
Crossflow Exp + Sim	500×500×5	m_{OA} = 1000 m^3/h (2 m/s), AFR = 33%	Nu: 3.66**	[85]
Crossflow & Counterflow Sim	500×500×34	V_{OA} = 2.4 m/s AFR = 50%	Nu: 4.12*	[86]
Counterflow Sim	500×100×5	V_{OA} = 2 m/s AFR = 33%	Nu: 7.54** U: 100	[52,87]
Two stages DEC+IEC Exp	890×600×0.025	m_{OA} = 0.1-0.2 kg/s	Nu: 150-450 U: 100-400	[88]
Crossflow Dry coil IEC Exp	400×400×2	m_{OA} = 800 m^3/h	U: 30	[89]
Semi-IEC (tubular) Sim	600×NA×0.015	m_{OA} = 140 m^3/h	U: 79.88	[90]

CrF: cross flow, CF: Counterflow, * Constant heat flux, **Constant surface temperature

A detailed investigation of heat transfer coefficient characteristics against important geometric and process parameters has been rarely conducted. Lin et al. [45] conducted an experiment and CFD-based investigation of heat transfer coefficients. For local temperature measurements, the IEC generic cell was equipped with 8 pairs of temperature sensors in dry and wet channels along the heat exchanger length. The local heat transfer coefficients for dry (h_d) and wet (h_w) channels were reported to be ranging between 25 and 30.3 W/m^2K as shown

in **Figure A-1 (a)**. The experimentation also showed minor irregular fluctuations in the heat transfer coefficients along the heat exchanger length. A similar trend for different outdoor air velocities (Figure A-1(b)) and outdoor air humidity (Figure A-1(c)) is also reported with small irregular variations in the heat transfer coefficient for dry and wet channels. The study also concluded that the heat transfer coefficients calculated using constant surface temperature and constant heat flux correlations resulted in an underestimation of the values. This is because the values calculated from experimentation were higher than the theoretically calculated values because of better heat transfer characteristics of the naturally formed boundary condition than the conventionally considered boundary conditions.

Similarly. Wan et al. [46] also investigated the characteristics of dry and wet side heat transfer coefficients for a counter-flow IEC. They reported that (refer to Figure A-1: Appendix A) h_d remained stagnant at 23.5 W/m^{2}K and h_w decreased from 22 to 20.5 W/m^{2}K when the channel length increased from 500 to 2000 mm. While both h_d and h_m decreased from 40 and 70 W/m^{2}K to 20 W/m^{2}K when the channel gap increased from 2 to 8. Similarly, with increasing outdoor air temperature from 38 to 40 °C (refer to Figure A-2: Appendix A) and outdoor air humidity 60 to 90%, the h_d remained constant at 20.5 W/m^{2}K, while the h_w decreased slightly from 23.5-22.5 W/m^{2}K. When the outdoor air velocity increased from 0.5 to 5 m/s, the h_d increased from 20.5 to 21.5 W/m^{2}K. While h_w remained almost insensitive to the outdoor air velocity. Meanwhile, with the increasing working air temperature from 20 to 26 °C, h_d remained constant at 20.5 W/m^{2}K while h_w increased from 22 to 24 W/m^{2}K. While, with increasing working air humidity from 40 to 70%, the h_d remained constant 20.5 W/m^{2}K while h_w decreased from 23 to 22 W/m^{2}K. Similarly, increasing working air velocity from 0.5 to 5 m/s increased h_w from 22 to 24 W/m^{2}K however, h_d remained constant at 20.5 W/m^{2}K. Another study by Min et al. [83] investigated the dry-side heat transfer coefficient under condensation in dry channel conditions. They showed that (refer to Figure A-3: Appendix A) The h_d increased from 100 to 270 W/m^{2}K when the velocity increased from 0.5 to 2.5 m/s.

3. Heat transfer coefficient correlation development

The methodology adopted here involves extending the existing dry channel heat transfer coefficient correlations by incorporating the effect of outdoor air temperature and the airflow rate ratio. In this regard, the wet side heat transfer coefficient is calculated using the Ranz and Marshall [37] correlation (refer to equation 1) which is reported to be one of the most accurate correlations for estimating heat transfer from water droplets as discussed above. While, for the dry side, three commonly used correlations (summarized as C1, C2, and C3 in Table 4) are

selected for comparison with the current experimental findings and the development of a new correlation.

Table 4.
Commonly used heat transfer coefficient correlations.

Type	Correlation	Ref.
Wet channel	$Nu_{WA} = 2 + 0.6\,\mathrm{Re}^{0.5}\,\mathrm{Pr}^{0.33}$	
Dry channel	$Nu_{C1} = 6.7932\,\mathrm{Re}_D^{0.0324}\,AFR^{-0.016}$	[45]
Dry channel	$Nu_{C2} = 8.235 + 0.0364\,\mathrm{Re}\,\mathrm{Pr}\,(D_h/L)$	[58]
Dry channel	$Nu_{C3} = \left[1.49\left(\frac{y}{D_h\,\mathrm{Re}\,\mathrm{Pr}}\right)^{4.5} + 8.235^{4.5}\right]^{1/4.5}$	[42,47–50]

3.1. Theoretical model

The dimensionless terms in the above correlations including the Reynolds, Prandtl, and Nusselt numbers can adequately capture the effect of geometric parameters and flow velocity to estimate the heat transfer in the channels. However, large variations in the outdoor air temperature and the airflow rate ratio can boost the heat transfer significantly which is not fully incorporated in the traditional correlations. Therefore, these correlations are revisited to capture these additional effects in the correlation.

The most important parameter for calculating the overall heat transfer coefficient is the total heat transferred or cooling capacity which is calculated using temperature drop (ΔT) across outdoor air, flow rate ($\dot{m}$), and the specific heat (c_p) as given below [52].

$$\dot{Q} = \dot{m}_{OA}\, c_{p,OA} \Delta T_{OA} = \dot{m}_{OA}\, c_{p,OA} \left(T_{OA,i} - T_{SA,o}\right) \tag{9}$$

Using log mean temperature difference (ΔT_{LMTD}), heat transfer area (A), and cooling capacity ($\dot{Q}_{OA}$) the overall heat transfer coefficient is calculated as [44] [91].

$$U = \frac{\dot{Q}}{A \Delta T_{LMTD}} \tag{10}$$

$$\Delta T_{LMTD} = \frac{\left(T_{OA,i} - T_{SA,o}\right) - \left(T_{SA,o} - T_{WA,i}\right)}{\ln\left(\frac{T_{OA,i} - T_{SA,o}}{T_{SA,o} - T_{WA,i}}\right)} \tag{11}$$

$$U = \frac{\dot{m}_{OA}\, c_{p,OA}\left(T_{OA,i} - T_{SA,o}\right)}{A\left\{\dfrac{\left(T_{OA,i} - T_{SA,\mathrm{o}}\right) - \left(T_{SA,\mathrm{o}} - T_{WA,i}\right)}{\ln\left(\dfrac{T_{OA,i} - T_{SA,\mathrm{o}}}{T_{SA,\mathrm{o}} - T_{WA,i}}\right)}\right\}} \tag{12}$$

Where the overall heat transfer coefficient is given as the convection heat transfer coefficients (h_{OA}, h_{WA}), and the conduction heat transfer through the wall is given as [92].

$$\frac{1}{U} = \frac{1}{h_{OA}} + \frac{t_{plate}}{k_{plate}} + \frac{1}{h_{WA}} \tag{13}$$

The wall resistance in the above equation is negligible because of the very small wall thickness (0.025 mm) and high thermal conductivity of Aluminum (i.e., 235 W/(m.K)). Therefore, the experimentation is focused on capturing the overall heat transfer coefficient. Then the experimental outdoor air heat transfer coefficient is calculated using the above equation. The correlation is then presented in the standard form of the Nusselt number which is given as:

$$Nu = \frac{h\, D_h}{k_{fluid}} \tag{14}$$

3.2. Experimentation

The experimental system considered in the study consists of an innovative indirect evaporative cooler as shown in Figure 1. The two major parts of the system include an air humidification (H) section and a sensible heat exchanger (SHX). The purpose of the humidification section is to supply working air to the heat exchanger at wet bulb temperature and 100% relative humidity. For this purpose, the high-temperature outdoor air is passed through the humidifier where it is cooled and humidified through continuous water mist showering (1-3). The fine mist boosts the air-water interaction mechanism in the humidifier thus producing cold humid air with additional mist particle carryover (3). The humidifier consists of a water sump, mist nozzles, a water pump, and a supplementary water supply through a float-controlled valve to the water sump. While the heat exchanger consists of alternative airflow channels dedicated to dry and working air streams. The dry air is taken as hot outdoor air in the dry channels which is sensibly cooled to the supply air temperature (1-2). While the heat from the dry channel is extracted by the working air stream in the wet channel (3-4). The mist particles in the working air are evaporated during the heat transfer process. Therefore, the mode of heat transfer in the working air channels includes both sensible and

latent heat transfer. The cold dry air is supplied to the room (2) and the hot humid working air is rejected by the environment (4). The operational scheme of the system is presented on the psychrometric chart in Figure 2.

(a)

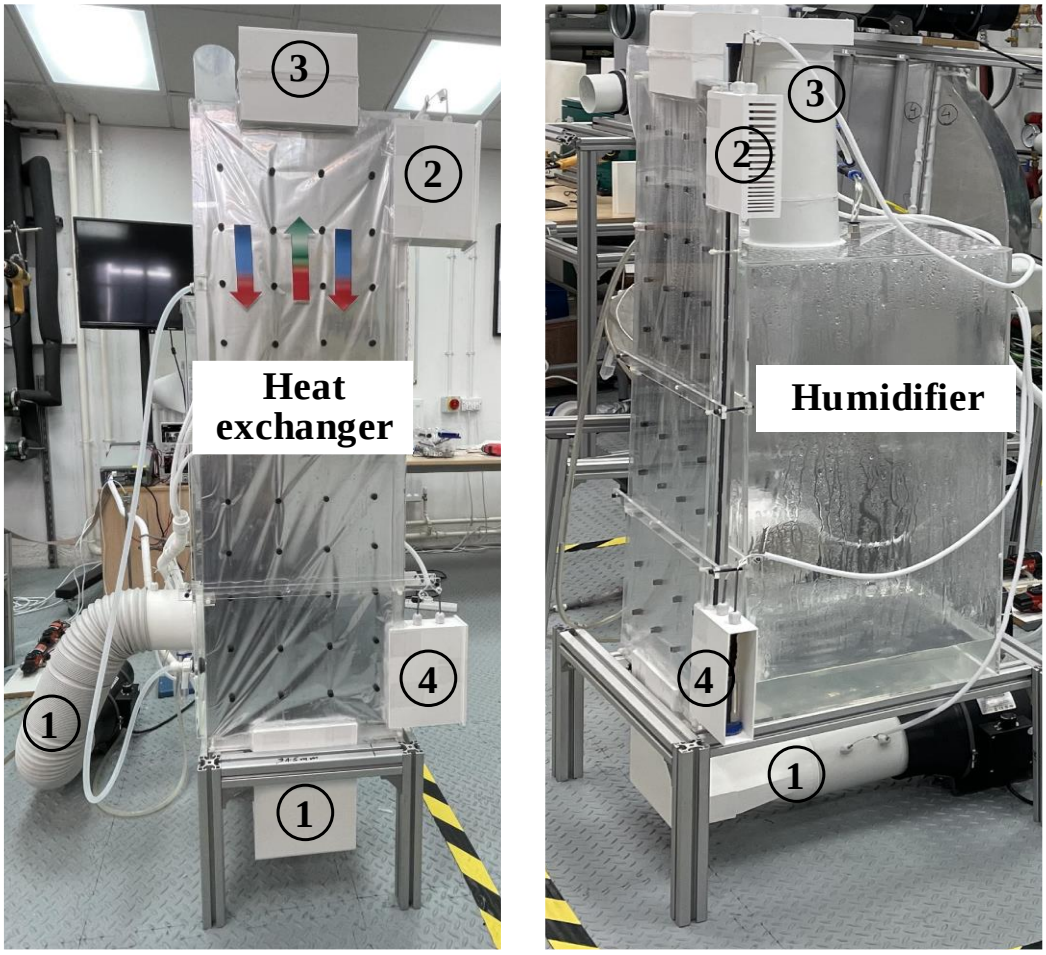

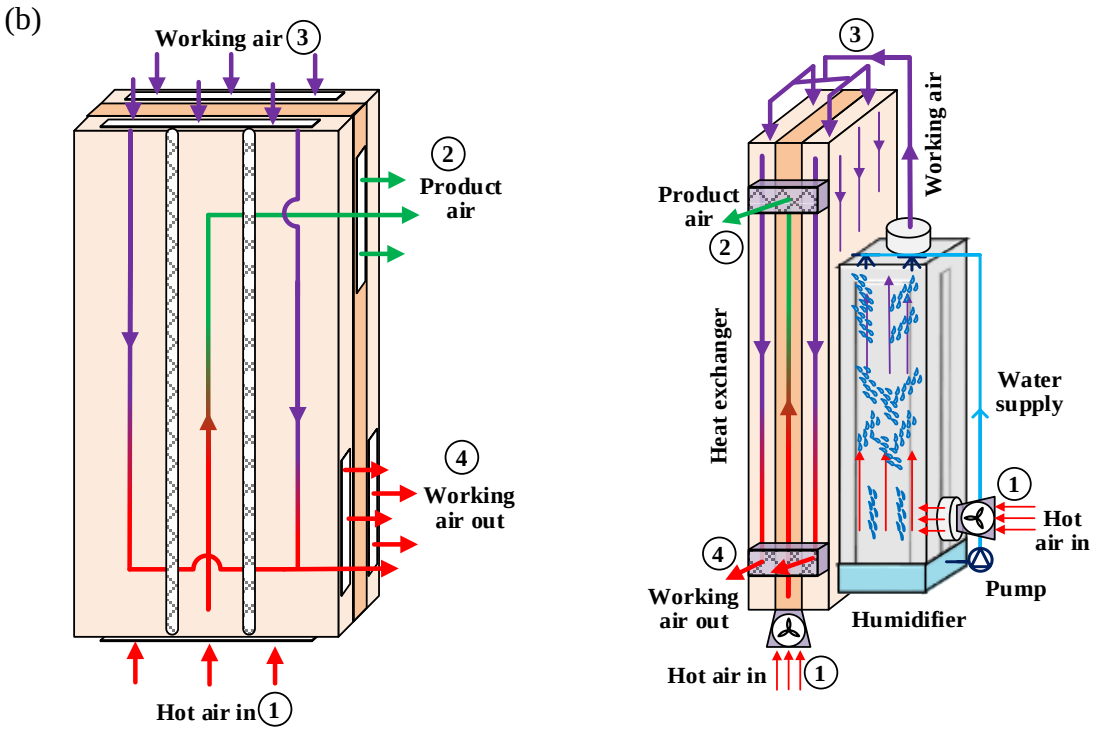

267 **Figure 2.** System pictorial view (a) front and side view of the experimental setup and (b)
268 schematic.

269

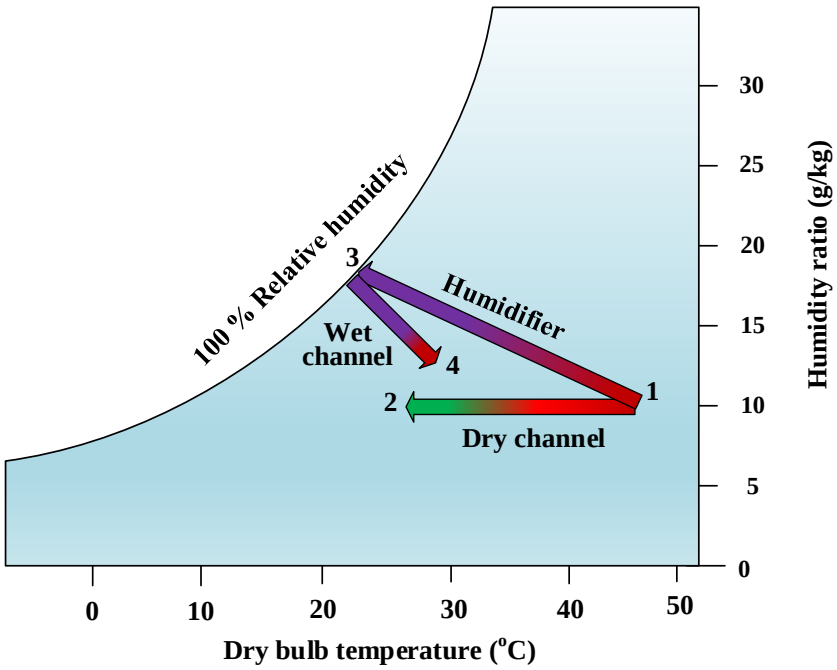

270

271 **Figure 3.** Proposed system psychrometric description.

272

273 The geometric specification of the system is summarized in Table 5. The system is fully
274 instrumented to capture all required data including dry bulb temperature, wet bulb temperature,

and velocity as presented in Table 6. For dry bulb temperature, the OMEGA thermistor probe with an accuracy of ±0.15 °C is used. While for wet bulb temperature, the customized wet bulb measuring station is used which involves a thermistor + Felt + Test tube. The dry and wet bulb temperature measurements are made at the dry channel inlet, dry channel outlet, humidifier inlet, humidifier outlet, wet channel inlet, wet channel outlet, and water sump. All the thermistors are connected to Agilent Benchlink Data Logger for real-time data monitoring and recording. For air flow rate measurement, hot-wire anemometer Testo 405i with an accuracy of ± 0.03 m/s is used at dry and wet channel outlets.

Table 5.
Summary of geometric and process parameters.

Parameter	**Value**
Humidifier dimensions, $H \times W \times L$, mm	800 × 400 × 400
Generic cell dimensions $H \times W \times \delta$, mm	1100 × 360 × 5
Aluminum sheet thickness, t_{AL}, mm	0.025
Number of channels, dry/wet	1/2
Outdoor air temperature at channel inlet, °C	25-50
Outdoor air humidity, ω, g/kg	10
Working air humidity at channel inlet, ω, g/kg	18
Outdoor air velocity, m/s	3
Air flow rate ratio	0.5-2.0

Table 6. Instrumentation details.

Parameter	**Sensor specification**	**Accuracy**
Temperature	Thermistors Company: OMEGA Measuring range: 0-80°C	± 0.15 °C
Humidity	Wet bulb measuring station Company: OMEGA Thermistor + Felt + Test tube	± 0.15 °C
Air velocity	Hot wire anemometer Company: Testo (model: 425i) Measuring range: 0 to 20 m/s	± 0.03 m/s

The experimentation involved system operation at assorted outdoor air and working air conditions to record the supply air temperature. For this purpose, the outdoor air and working

temperature varied between 27 to 50 °C, and the airflow rate ratio was from 50% to 200%. It covers the whole range of outdoor air temperatures to appropriately incorporate the effect. Since last decade the peak temperature during summer is > 45 °C in most parts of GCC and Asia which are the biggest markets of the cooling industry. Moreover, most of the earlier IEC systems are tested in labs and onsite testing is seldom seen so they are limited to < 42 °C. So, to enhance the applicability of the current study and correlation over a wider range the temperature. Moreover, the evaporative cooling system performance is influenced by the outdoor air temperature, flow velocity, and airflow rate ratio. For each data set the experimental procedure is the same as the system is first operated to achieve the required outdoor air temperature at the dry channel inlet and the humidifier inlet. Then the water showering in the humidifier starts to achieve the wet bulb temperature at the wet channel inlet. Once the system temperatures achieve a steady state trend the data is used for subsequent calculations like cooling capacity, efficiency, coefficient of performance, and the heat transfer coefficient.

Meanwhile, it is worth mentioning that the data in this study is presented against dry bulb temperature because of the extensive application of evaporative cooling systems for dry and hot climates. Though in IEC systems the supply air humidity is constant as that of the inlet, under extremely high outdoor humidity conditions the outdoor air needs to be dehumidified. This is because the evaporative system performance drops under humid conditions and the thermal comfort is not achieved with high humidity supply air. In such cases, the IEC system is integrated with a dehumidifier (desiccant wheel, microwave, membrane-based, etc.). This integration increases the energy consumption of the system; however, the overall COP is still higher than MVC systems. It is also important to mention that the dehumidification technologies are well established and have been extensively used for domestic and industrial air treatment. However, the scope of this study is only limited to IEC sections.

4. Results and discussion

The most important parameters that govern the heat transfer coefficient in the heat exchanger are cooling capacity and log mean temperature difference (LMTD). A comprehensive summary of the parameters used in the experimental data is presented in **Table *7***. The uncertainty study is conducted at 45 ℃ using the accuracy of the sensors and anemometer. The maximum uncertainty in the estimation of different parameters is as follows: cooling capacity ± 2.13, log mean temperature difference ± 0.314, and overall heat transfer coefficient ± 1.71. An energy balance diagram of the heat exchanger as presented in Figure 4. It is important to note that the cooling in the dry channel is produced by rejecting heat to the wet channel. The heat in the wet channel is transferred in sensible and latent forms. However, latent heat has a major share in the wet channel because of evaporation. However, an increase in the working air temperature shows sensible heat transfer as well. The contribution of sensible and latent heat transfer is presented in Table 8.

Table 7.
Summary of experimental data.

AFR (%)	$T_{OA,i}$ (℃)	$T_{SA,o}$ (℃)	$T_{WA,i}$ (℃)	$T_{WA,o}$ (℃)	LMTD (℃)	Q_{Total} (W)	$Q_{Sensible}$ (W)	Q_{Latent} (W)	U W/(m^2.K)
200	50	25.47	23.86	25.86	8.36	178.46	13.32	165.15	30.31
	45	24.86	23.65	25.19	6.72	147.91	10.27	137.64	31.24
	40	23.86	22.89	24.05	5.42	118.81	7.66	111.16	31.19
	35	22.91	22.02	22.68	4.39	88.41	4.41	84.00	28.57
	30	21.55	20.58	21.26	3.60	62.96	4.51	58.45	24.84
	25	20.52	19.54	20.24	2.40	32.55	4.70	27.85	19.22
150	50	26.97	23.29	25.69	10.98	167.86	15.98	151.88	21.71
	45	26.99	23.74	25.77	9.03	131.13	13.46	117.67	20.62
	40	26.04	23.87	25.02	6.67	102.02	7.67	94.35	21.73
	35	25.16	23.57	24.17	4.88	72.82	4.02	68.80	21.16
	30	23.52	21.98	22.67	3.70	46.90	4.56	42.35	17.97
	25	21.92	20.85	21.36	2.05	21.33	3.40	17.93	14.76
100	50	28.08	21.62	29.3	12.24	158.81	50.96	107.85	18.42
	45	27.42	22.08	28.15	10.08	128.61	40.31	88.30	18.10
	40	26.26	22.21	26.71	7.82	100.15	29.83	70.33	18.19
	35	24.86	21.64	25.02	6.10	76.06	22.47	53.59	17.69
	30	22.93	20.60	22.79	4.33	51.41	14.52	36.89	16.86
	25	21.55	19.93	21.30	2.54	25.42	9.13	16.30	14.17
50	50	32.26	23.20	29.58	14.03	129.53	42.37	87.16	13.11
	45	31.38	23.93	29.10	11.19	99.31	34.36	64.94	12.60

	40	29.78	24.09	27.92	8.49	73.91	25.40	48.51	12.36
	35	28.10	23.94	26.45	6.28	53.23	16.76	36.47	12.04
	30	25.41	22.51	24.48	4.34	37.89	13.10	24.79	12.40
	25	23.17	21.75	22.79	1.98	16.59	6.87	9.73	11.87

331

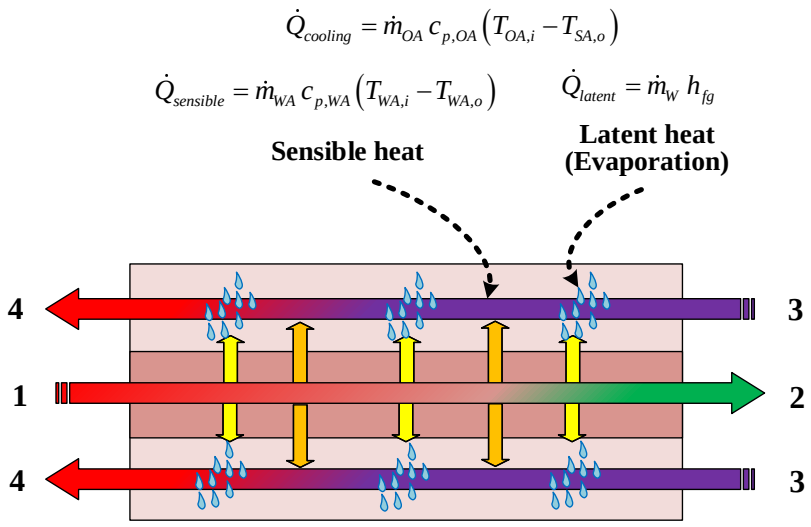

332

333 **Figure 4.** Energy balance diagram for heat exchanger.

334 The effect of outdoor air temperature and airflow rate ratio on the cooling capacity
335 calculated experimentally is presented in Figure 5. It shows that the cooling capacity is
336 significantly influenced by outdoor air temperature as well as the airflow rate ratio. For
337 instance, a maximum cooling capacity of 178 W is achieved at an AFR of 200% and an outdoor
338 air temperature of 50 °C. While the minimum cooling capacity of 178 W is achieved at an AFR
339 of 50% and an outdoor air temperature of 25 °C. This is because at higher outdoor air
340 temperatures the temperature differential across dry and wet channels is considerably high. The
341 working air always enters at the wet bulb temperature which boosts the heat transfer process
342 and cooling capacity at higher outdoor air temperatures. Similarly, at higher air flow rate ratios,
343 the mist carry-over in the working air channels is increased which enhances the evaporation
344 and increases the latent heat extraction. Overall, the higher temperature and higher air flow rate
345 ratio increase the heat transfer rate. Meanwhile, Figure 6 shows that the maximum LMTD is
346 obtained at higher outdoor temperatures and lower air flow rate ratios. This is because at higher
347 AFR the latent heat transfer dominates, and the temperature rise in the working air outlet stream
348 becomes smaller. The corresponding overall heat transfer coefficient values at different
349 outdoor air temperatures and AFR are presented in Figure 7.

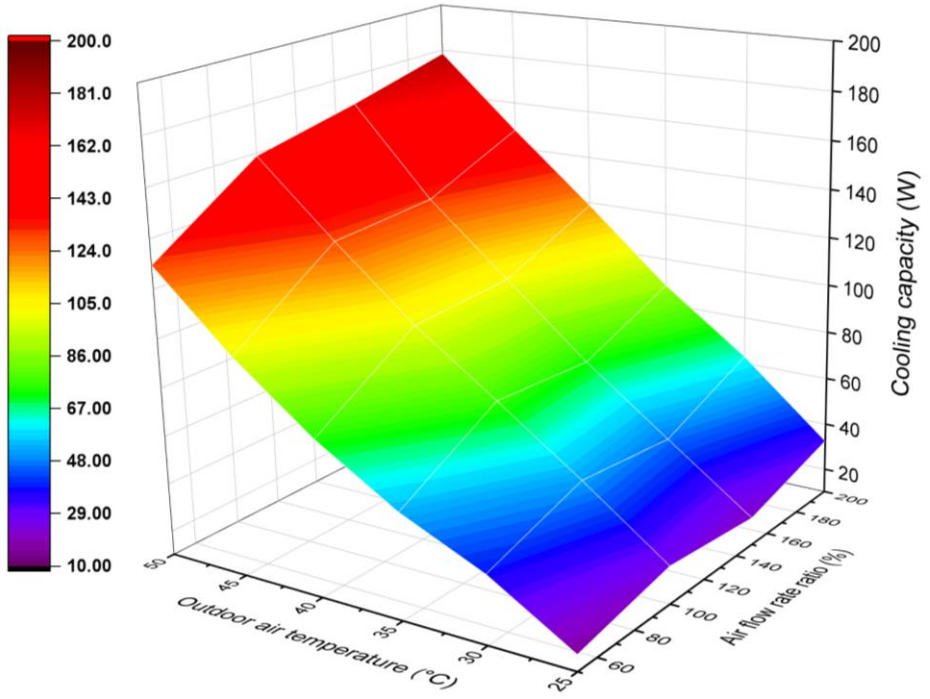

350

351 **Figure 5.** Cooling capacity variations versus T_{OA} and AFR.

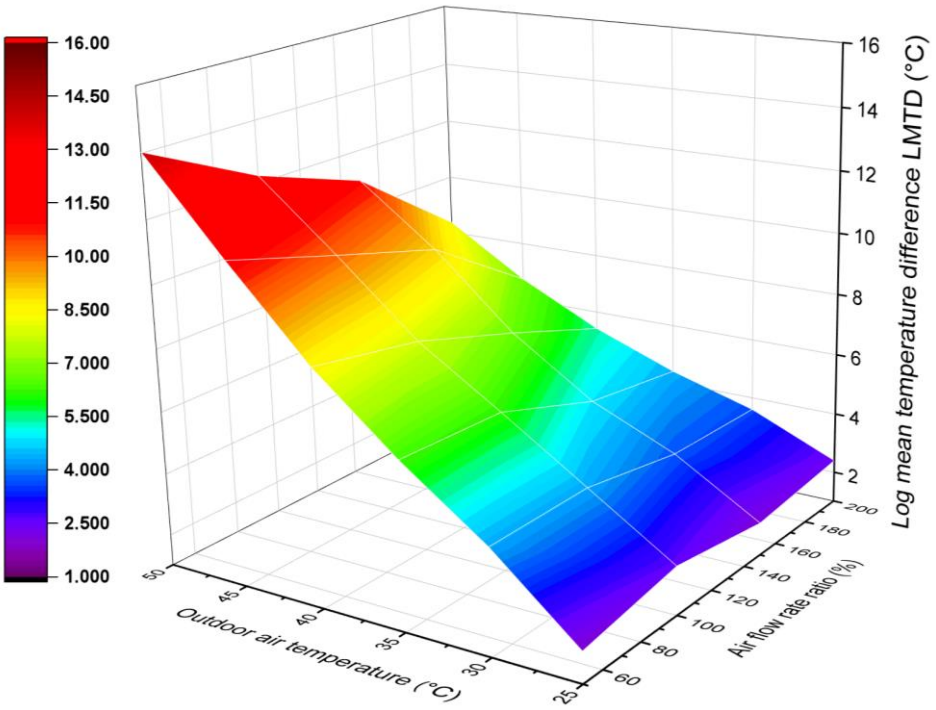

352

353 **Figure 6.** Log means temperature difference versus T_{OA} and AFR.

354

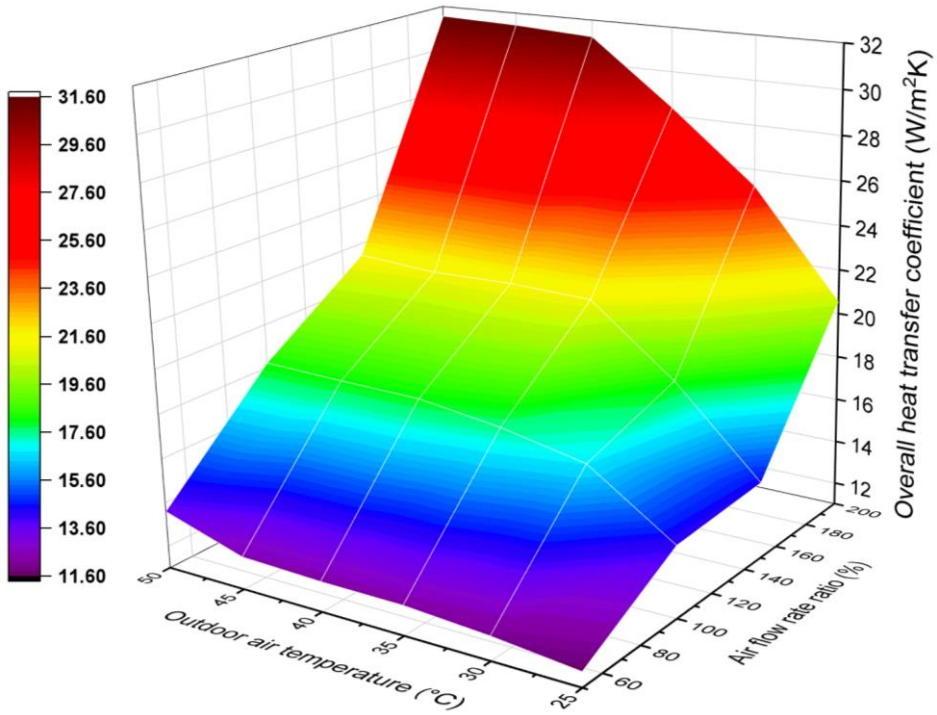

Figure 7. Overall heat transfer coefficient versus T_{OA} and AFR.

The trends for experimental overall heat transfer coefficients calculated using cooling capacity and log mean temperature difference are presented in Figure 8. Figure 8(a) presents the overall heat transfer coefficient at different outdoor air conditions for an air flow rate ratio of 50%. It is observed that the U value increased by 11% from 11.2 W/m^{2}K to 12.5 W/m^{2}K when the outdoor air temperature increased from 25 °C to 50 °C. Meanwhile, for AFR of 100% as shown in Figure 8(b) shows that the U value increased by 27.6% from 14.1 W/m^{2}K to 17.92 W/m^{2}K for the same outdoor air temperature variation from 25 °C to 50 °C. Similarly, for AFR of 150% the U values increase by 45% from 14.6 W/m^{2}K to 21.3 W/m^{2}K (refer to Figure 8(c)) and for 200% (refer to Figure 8(d)) by 55% from 20.1 W/m^{2}K to 31.6 W/m^{2}K for the outdoor air temperature varying from 25 °C to 50 °C. It is worth mentioning that the conventional IEC system water flows inside the wet channel and the heat transfer coefficient is majorly governed by the flow rate of air and water. The effect of these parameters is incorporated in terms of Reynold number and Pr number. In the proposed cooler, fine water droplets are only carried with mist and evaporation takes place in the wet channel from these water mist particles. The variation in outdoor air temperature enhances the temperature differential across the air streams in dry and wet channels. It enhances the rate of orthogonal heat transfer between the channels. This increase in heat transfer with outdoor air temperature can be seen in the cooling capacity which is then used to calculate the heat transfer coefficient

experimentally. Without incorporating the effect of outdoor air temperature, the heat transfer coefficient gives poor estimation which is only sufficient for lower operating temperature where the effect is insignificant.

Overall, the heat transfer coefficient is influenced by outdoor air temperatures and airflow rate ratio. The variations are significantly enhanced at higher values of temperature and airflow rate ratio. These variations are because higher outdoor air temperature increases temperature differential and a higher air flow rate ratio boosts evaporation which in turn enhances the heat transfer.

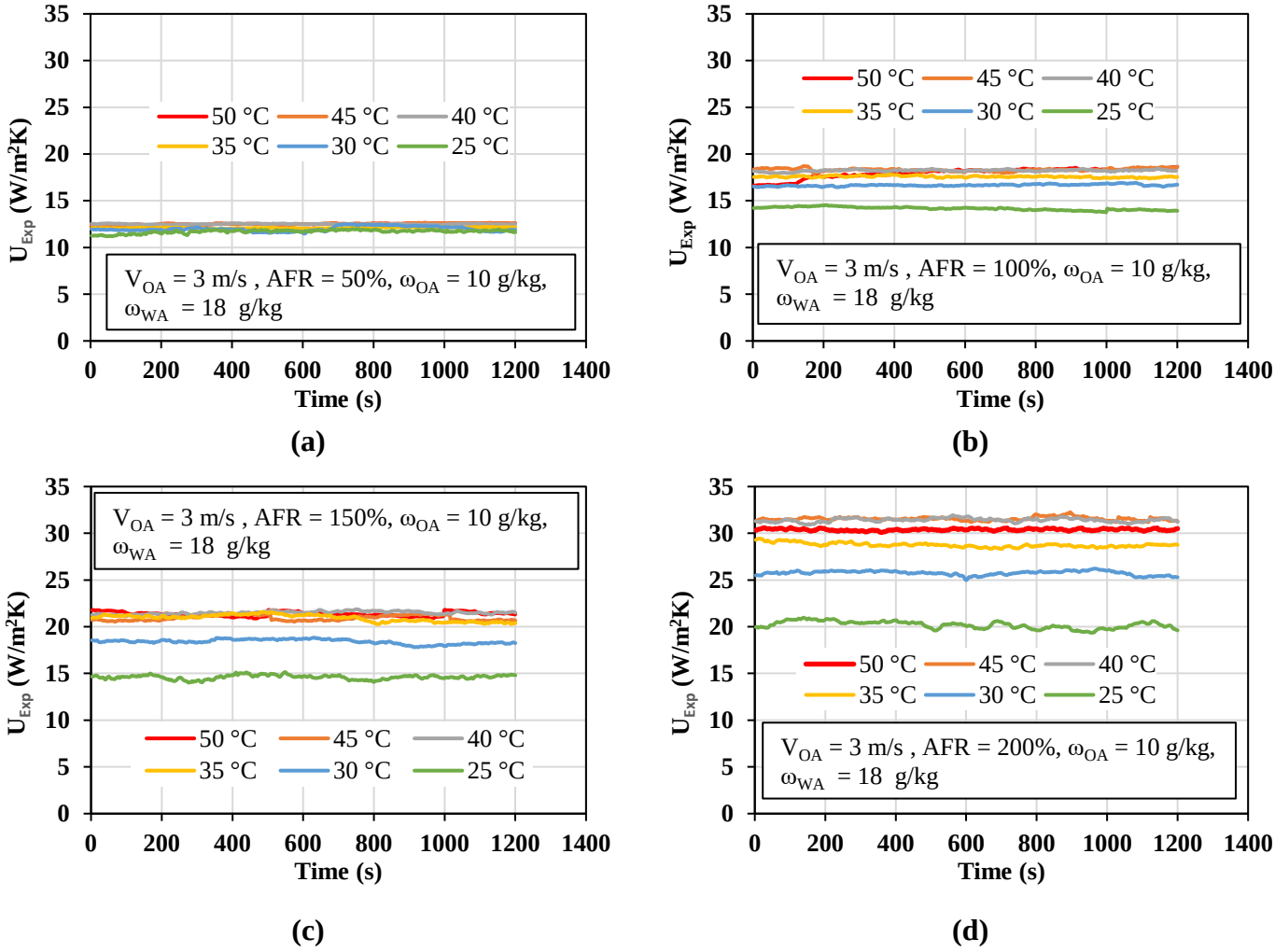

Figure 8. Overall heat transfer coefficient trends at different T_{OA} and AFR of (a) 50%, (b) 100%, (c) 150%, and (d) 200%.

The above analysis shows that the heat transfer coefficient is strongly influenced by outdoor air temperature and airflow rate ratio. Therefore, the correlations calculating the local heat transfer coefficients are required to incorporate the effect of these parameters. Meanwhile, the

traditional heat transfer coefficient correlations in literature for dry channels are based on simple airflow between parallel plates with major reliance on Re and Pr numbers as shown in Table 4. These can adequately incorporate the effect of geometric parameters, flow parameters, and thermophysical properties in the respective channel. However, the effect of heat transfer enhancement due to variations in outdoor air temperature and evaporation (in wet channels) is not covered. Therefore, the values of dry side local heat transfer coefficients calculated using traditional correlations (presented in Table 4 as C1, C2, C3) from literature remain insensitive to the outdoor air temperature and airflow rate ratio as shown in Figure 9. It shows that the h_{OA} values calculated using these correlations remain almost constant at 22-23 W/m^{2}K for all outdoor air temperatures and airflow rate ratios. On the other hand, the experimental values show significant variations from 16 to 57 W/m^{2}K against T_{OA} and AFR. It implies that the effect of outdoor air temperature and airflow rate ratio is not properly captured in traditional correlations. This is because the effect of temperature in these correlations only occurs in Re and Pr numbers due to thermophysical properties like density (ρ), viscosity (μ), thermal conductivity (k), specific heat (C_p), etc. Meanwhile, it is important to emphasize that these properties are a weak function of temperature with benign variation over temperature ranging from 25 to 50 °C as shown in Figure 10. Therefore, traditional correlation does not incorporate these effects and necessitates the development of new correlations addressing these limitations.

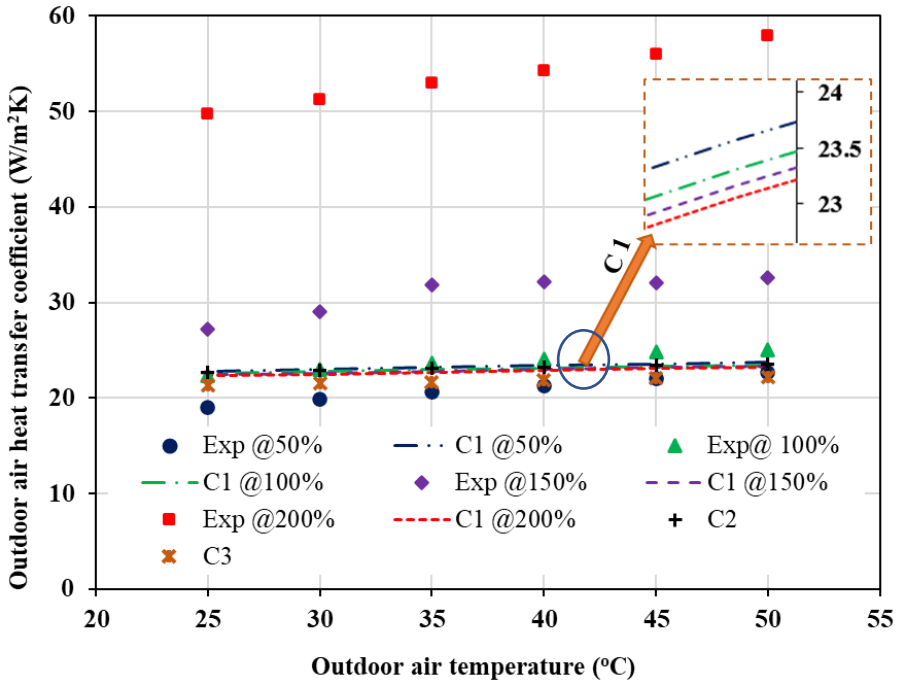

Figure 9. Heat transfer coefficient comparison between experimental data and literature correlations from Table 4 as C1 [45], C2 [58], C3 [42].

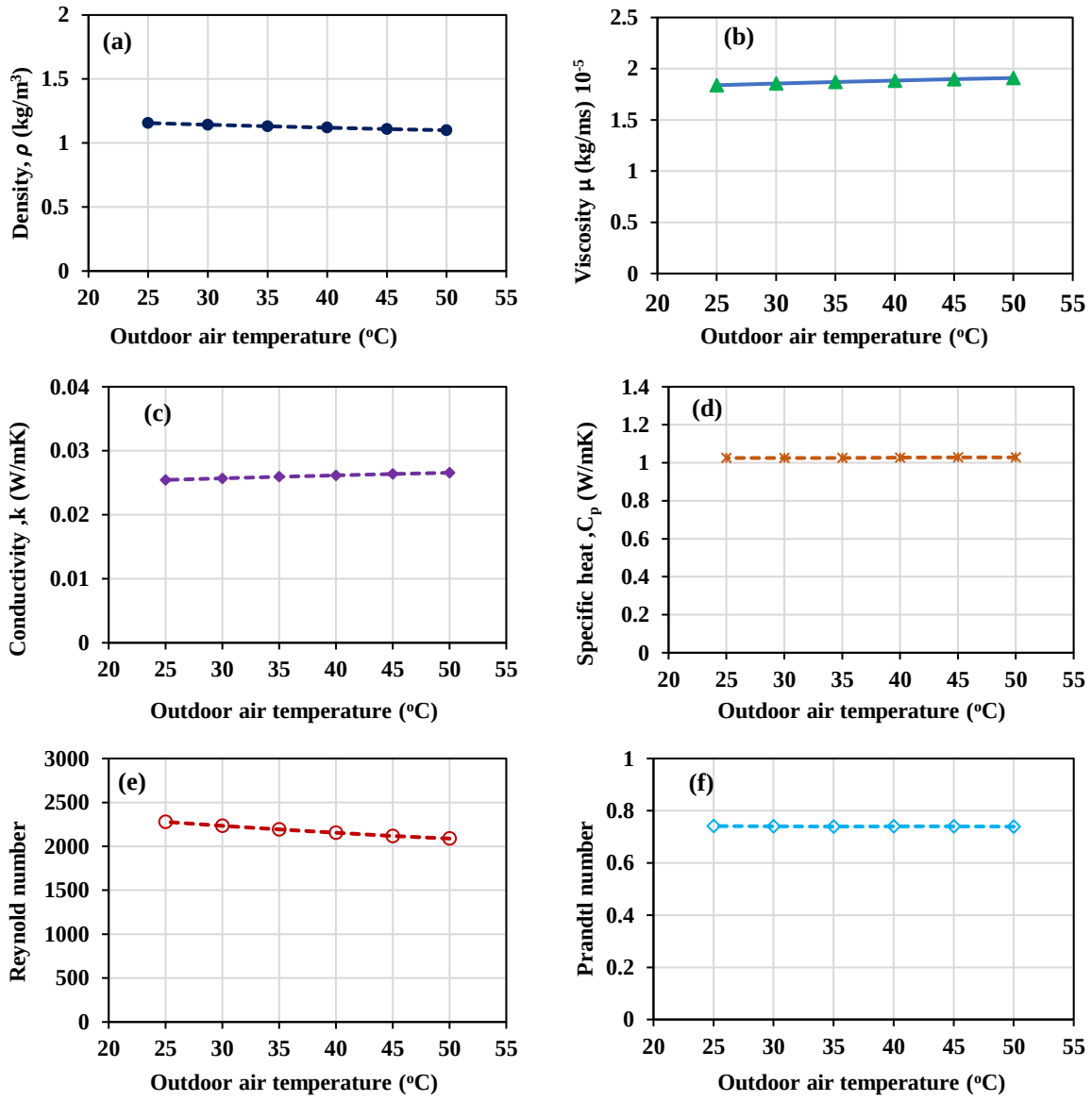

412 **Figure 10.** Thermophysical properties variation with temperature for dry air.

413

414 A correlation based on new experimental measurements incorporating the additional effects of
415 air flow rate ratio (AFR) and outdoor air temperature (T_{OA}) is proposed for the calculation of
416 the heat transfer coefficient. The correlation is formulated in terms of key parameters including
417 Reynold number (Re), Prandtl number (Pr) air flow rate ratio (AFR), and outdoor air
418 temperature (T_{OA} (K)) normalized by reference temperature T_{ref} (K) as given below.

419 $$Nu_{OA} = \frac{h_{OA} D_h}{k} = 8.235 + 0.63\,\mathrm{Re}^{0.047}\,\mathrm{Pr}^{0.89}\,\overbrace{AFR^{4.29}\left(\frac{T_{OA}}{T_{ref}}\right)^{2.61}}^{\text{Newly introduced terms}} \quad (15)$$

A regression with these parameters against the experimental results is conducted as presented in Figure 11. It shows a good agreement with R^2 = 0.99 between experimental and calculated (from the proposed correlation) values. A slightly higher discrepancy between experimental and correlation values is observed at lower (i.e., 25 °C) outdoor air temperatures. This is because the system cooling capacity is significantly decreased than the designed value at this temperature. Moreover, the IEC systems are not generally operated in this temperature range because of being in the ASHRAE comfortable zone. Therefore, the proposed correlation can be used with acceptable accuracy for IEC operation at as high as 50 °C temperature. The correlation plot for the proposed formulation showing dependency on different parameters is presented in Figure 12. It shows that the most influential parameters are air flow rate ratio with a significance level of 0.87, followed by outdoor air temperature with 0.23, and then Prandtl number with 0.23 and Reynold number with 0.037. It affirms the dependency of correlation on the newly added terms.

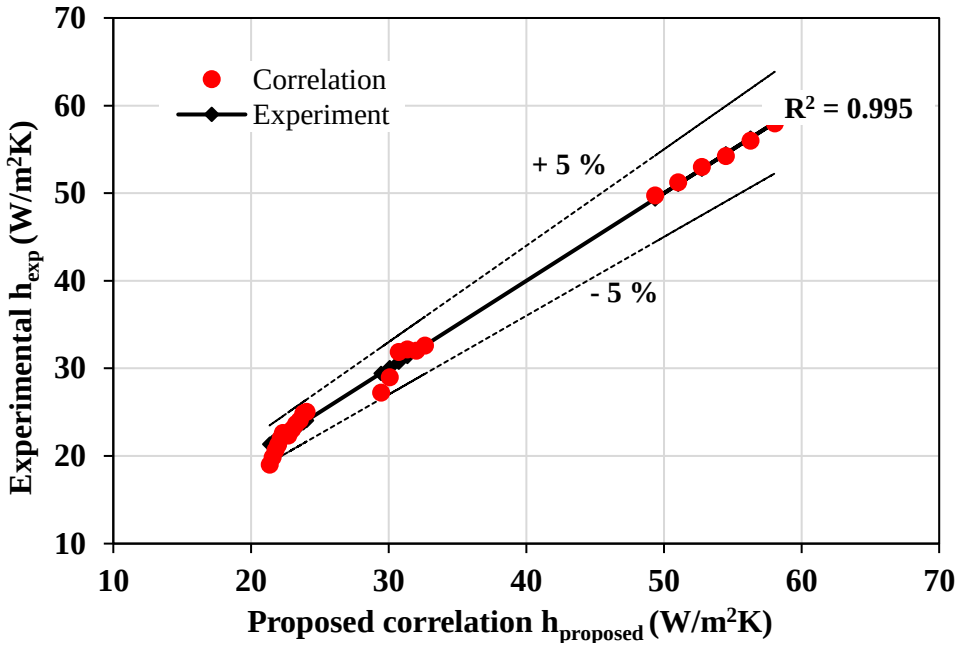

Figure 11. Correlation validation with experimental data.

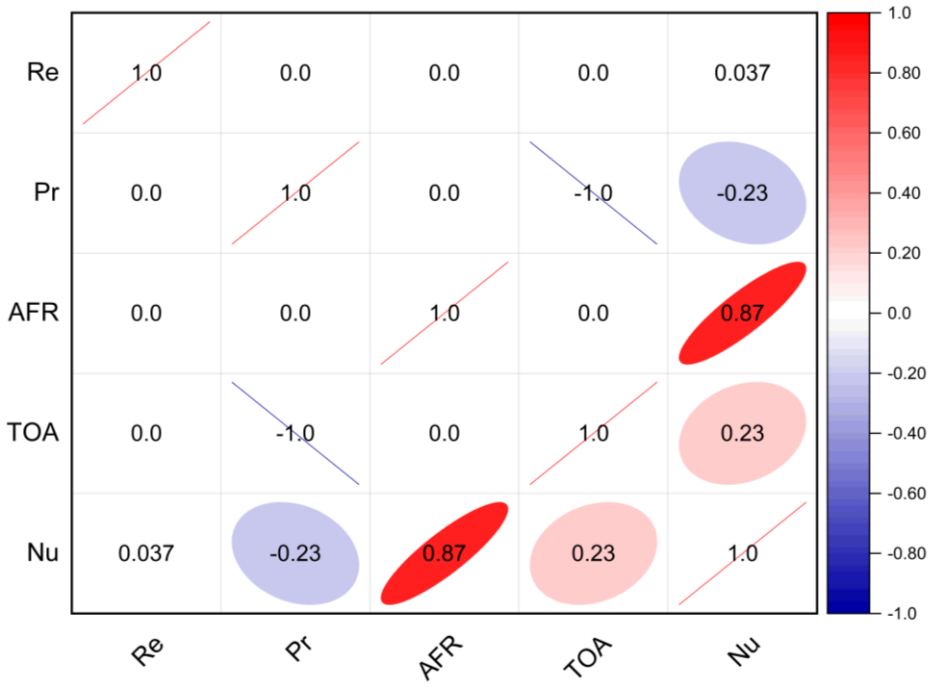

Figure 12. Correlation coefficient plot for parameters.

Figure 13 and Figure 14 show a comparison of the outdoor air heat transfer coefficient calculated using the proposed correlation and measured experimentally. It shows that the proposed correlation can effectively capture the effect of outdoor air temperature and airflow rate ratio. Therefore, the calculated values occur within ± 5% of the experimental values. Particularly, at higher outdoor air temperatures and higher air flow rate ratios where the effects are dominant, the accuracy of the correlation is higher. Moreover, the earlier studies in the literature are only limited to a maximum outdoor air temperature of 42 °C. While the current study incorporates the outdoor air temperature of as high as 50 °C which makes the proposed correlation suitable for IEC system design under harsh climatic conditions.

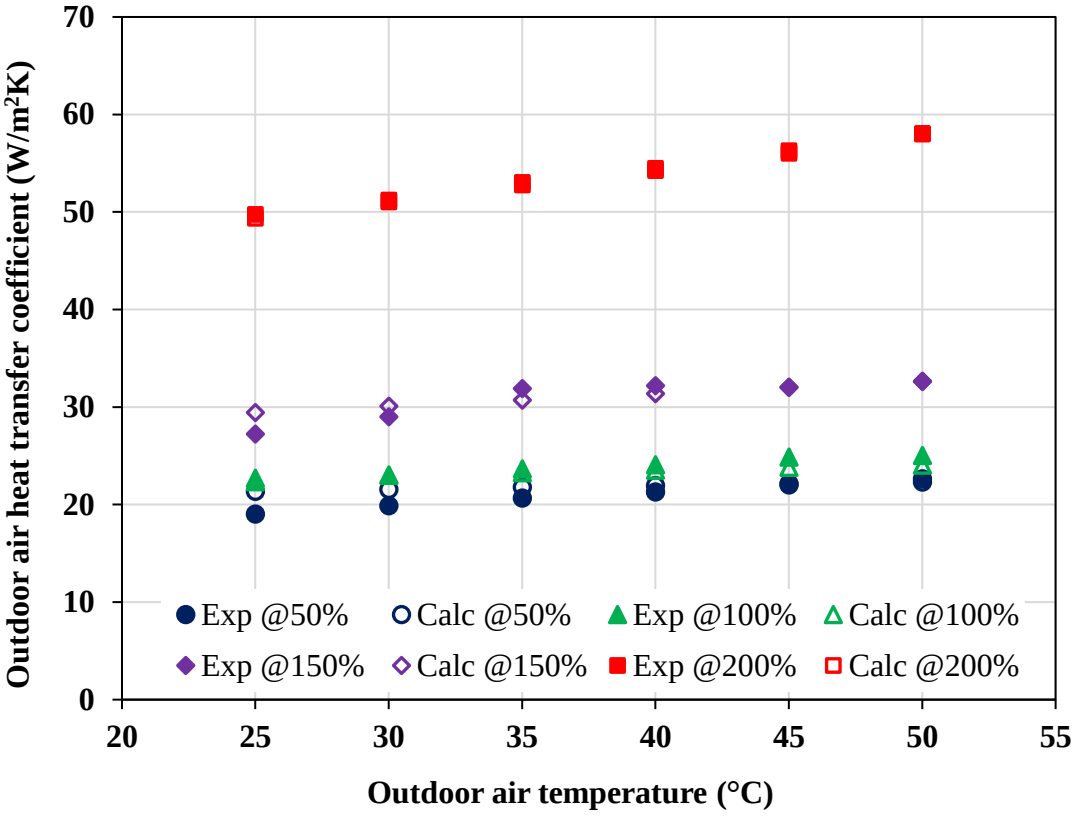

447

448 **Figure 13.** Comparison of experimental and proposed correlation heat transfer coefficient
449 values.

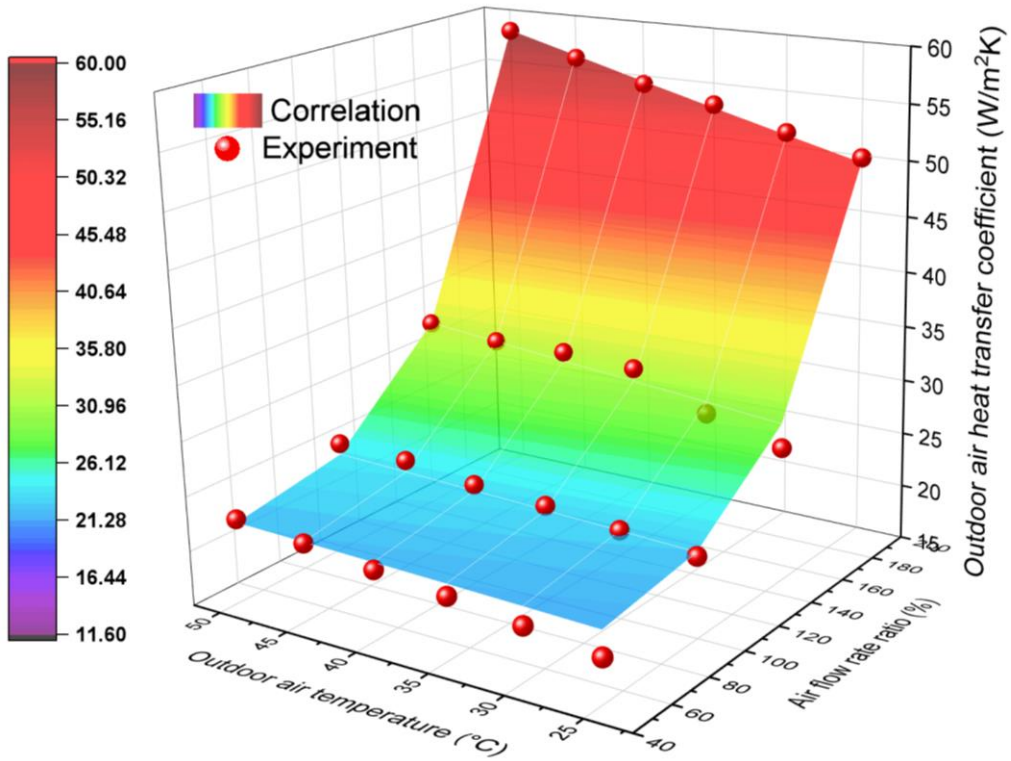

450

451 **Figure 14.** 3D surface distribution of the h values for the experiment and correlation.

5. Conclusion

Indirect evaporative cooling technology is a sustainable alternative to conventional cooling systems in hot dry climatic areas. A novel indirect evaporative cooler addressing major limitations in the earlier systems is proposed and developed in this study. The study is particularly focused on the development of a dry channel heat transfer coefficient for the large-scale expansion of these systems. This is because the conventional correlations are observed to be insensitive to these parameters and give a poor prediction of the heat transfer coeffects. Predominantly, at higher values of outdoor air temperature and working air flow rate the conventional correlations become inapplicable and mislead the calculations. The major findings of this study are summarized below.

- The proposed system achieved a temperature drop up to 25 ℃, and a cooling capacity of 178 W. The system showed higher performance under higher outdoor air temperatures because of a larger temperature differential across channels.
- The dry side heat transfer was calculated using conventional correlation hover around 22-23W/m^2K for the outdoor air temperatures varying between 25 to 50 ℃ and air flow rate ratios of 50% to 200%.
- The experimental and proposed correlation heat transfer coefficient value varied from 16 to 57 W/m^2K when the outdoor air temperature increased from 25 to 50 ℃ and the air flow rate ratio increased from 50 to 200%.
- The most influential parameters in indirect evaporative cooler design are observed to be Reynold number, Prandtl number, air flow rate ratio, and outdoor air temperature under hot dry climates.
- The newly developed heat transfer correlation properly incorporates the effect of outdoor air temperature ranging from 25-50 ℃ and air flow rate ratio ranging from 50-200% with an accuracy of ±5% with the experiment.

Overall, the conventional correlations underpredict the heat transfer coefficient values and are unable to track the effect of outdoor air temperature and airflow rate ratio. So, the new terms are introduced in the proposed correlation that captures the effect of temperature and airflow rate ratio. Moreover, the high experimental accuracy makes the proposed correlation viable for the future design of IEC systems over assorted operating scenarios.

Acknowledgment

The authors would like to thank Northumbria University UK for funding under reference #RDF20/EE/MCE/SHAHZAD, and Northern Accelerator Proof-of-Concept award for AD4DCs (NACCF-232) Awarded to Dr. Muhammad Wakil Shahzad. Also acknowledged is the support provided by the KAUST cooling initiative (REP/1/3988-01-01). This work was supported by the UK Engineering and Physical Sciences Research Council (EPSRC) [grant number EP/R045518/1]. For Open Access, the authors have applied a CC BY public copyright license to any Author Accepted Manuscript version arising from this submission.

Nomenclature

A	Area, m^2
c_p	Specific heat, J/(kg.K)
D_h	Hydraulic diameter, m
Gz	Graetz number
h	heat transfer coefficient, W/(m^2.K)
k	Thermal conductivity, W/(m.K)
L	Length, m
$\dot{m}$	Mass flow rate, kg/s
Nu	Nusselt number
Pr	Prandtl number
$\dot{Q}$	Cooling capacity, W
Re	Reynolds number
Sh	Sherwood number
T	Temperature, °C
t	Thickness, mm
U	Overall heat transfer coefficient, W/(m^2.K)
V	Velocity, m/s

Greek letters

Δ	Change in quantity
ω	Humidity, g/kg
μ	Viscosity, kg/(m.s)
ρ	Density, kg/m^3

Subscripts

Exp	Experimental

LMTD	Log mean temperature difference
OA	Outdoor air
ref	Reference
SA	Supply air
WA	Working air

Abbreviations

AC	Air conditioning
AFR	Air flow rate ratio
CFD	Computational fluid dynamics
COP	Coefficient of performance
IEC	Indirect evaporative cooler
OA	Outdoor air
RH	Relative humidity, %
TWh	Terawatt hours
WA	Working air

493

494

References

[1] IPCC. Climate change 2014 synthesis report. vol. 978-92–916. 2014. https://doi.org/10.1017/CBO9781139177245.003.

[2] Campbell BI, Kalanki A, Sachar S, Hartley B. Solving the Global Cooling Challenge: How to Counter the Climate Threat from Room Air Conditioners. 2018.

[3] IEA. The Future of Cooling: Opportunities for energy-efficient air conditioning 2018:92. https://www.iea.org/data-and-statistics/charts/global-air-conditioner-stock-1990-2050 (accessed July 9, 2021).

[4] Amasyali K, El-Gohary NM. A review of data-driven building energy consumption prediction studies. Renew Sustain Energy Rev 2018;81:1192–205. https://doi.org/10.1016/j.rser.2017.04.095.

[5] Dino GE, Palomba V, Nowak E, Frazzica A. Experimental characterization of an innovative hybrid thermal-electric chiller for industrial cooling and refrigeration application. Appl Energy 2021;281:116098. https://doi.org/10.1016/j.apenergy.2020.116098.

[6] Howarth N, Odnoletkova N, Alshehri T, Almadani A, Lanza A, Patzek T. Staying Cool in A Warming Climate: Temperature, Electricity and Air Conditioning in Saudi Arabia. Climate 2020;8:4. https://doi.org/10.3390/cli8010004.

[7] Air conditioning use emerges as one of the key drivers of global electricity-demand growth - News - IEA 2018. https://www.iea.org/news/air-conditioning-use-emerges-as-one-of-the-key-drivers-of-global-electricity-demand-growth (accessed January 23, 2021).

[8] Paupardin SE. Is the world facing a looming cold crunch 2019. https://www.sageglass.com/eu/visionary-insights/world-facing-looming-cold-crunch (accessed April 8, 2021).

[9] Li J, Liu Y, Zhang R, Liu Z, Xu W, Qiao B, et al. Load distribution of semi-central evaporative cooling air-conditioning system based on the TRNSYS platform. Energies 2018;11. https://doi.org/10.3390/en11051186.

[10] Ham SW, Jeong JW. DPHX (dew point evaporative heat exchanger): System design and performance analysis. Energy 2016;101:132–45. https://doi.org/10.1016/j.energy.2016.02.019.

[11] Jani DB, Mishra M, Sahoo PK. Solid desiccant air conditioning - A state of the art review. Renew Sustain Energy Rev 2016;60:1451–69. https://doi.org/10.1016/j.rser.2016.03.031.

[12] Kim MH, Park JY, Park JS, Jeong JW. Application of desiccant systems for improving the performance of an evaporative cooling-assisted 100% outdoor air system in hot and humid climates. J Build Perform Simul 2015;8:173–90. https://doi.org/10.1080/19401493.2014.899395.

[13] Amer O, Boukhanouf R, Ibrahim HG. A Review of Evaporative Cooling Technologies. Int J Environ Sci Dev 2015;6:111–7. https://doi.org/10.7763/ijesd.2015.v6.571.

[14] Jain JK, Hindoliya DA. Experimental performance of new evaporative cooling pad materials. Sustain Cities Soc 2011;1:252–6. https://doi.org/10.1016/j.scs.2011.07.005.

[15] Khobragade NN, Kongre SC. Experimental Performance of Different Evaporative Cooling Pad Material of Direct Evaporative Cooler in Hot and Dry Region. Int J Innov Technol Res 2016;4:2920–3.

[16] Laknizi A, Mahdaoui M, Ben Abdellah A, Anoune K, Bakhouya M, Ezbakhe H. Performance analysis and optimal parameters of a direct evaporative pad cooling system under the climate conditions of Morocco. Case Stud Therm Eng 2019;13:100362. https://doi.org/10.1016/j.csite.2018.11.013.

[17] Kashyap S, Sarkar J, Kumar A. Proposal and month-wise performance evaluation of a novel dual-mode evaporative cooler. Heat Mass Transf 2019;55:3523–36. https://doi.org/10.1007/s00231-019-02670-6.

[18] Baakeem SS, Orfi J, Mohamad A, Bawazeer S. The possibility of using a novel dew point air cooling system (M-Cycle) for A/C application in Arab Gulf Countries. Build Environ 2019;148:185–97. https://doi.org/10.1016/j.buildenv.2018.11.002.

[19] Baakeem SS, Orfi J, Mohamad AA. Investigations of geometrical and operational aspects of a dew-point air-cooling system (M-cycle). J Build Eng 2021;36:102117. https://doi.org/10.1016/j.jobe.2020.102117.

[20] Liu Q, Guo C, Ma X, You Y, Li Y. Experimental study on total heat transfer efficiency evaluation of an indirect evaporative cooler. Appl Therm Eng 2020;174:115287. https://doi.org/10.1016/j.applthermaleng.2020.115287.

[21] Shahzad MW, Lin J, Xu B Bin, Dala L, Chen Q, Burhan M, et al. A spatiotemporal indirect evaporative cooler enabled by transiently interceding water mist. Energy 2021;217:119352. https://doi.org/10.1016/j.energy.2020.119352.

[22] Oh SJ, Shahzad MW, Burhan M, Chun W, Kian Jon C, KumJa M, et al. Approaches to energy efficiency in air conditioning: A comparative study on purge configurations for indirect evaporative cooling. Energy 2019;168:505–15. https://doi.org/10.1016/j.energy.2018.11.077.

[23] Min Y, Chen Y, Yang H. A statistical modeling approach on the performance prediction of indirect evaporative cooling energy recovery systems. Appl Energy 2019;255:113832. https://doi.org/10.1016/j.apenergy.2019.113832.

[24] Pedrazzi S, Allesina G, Muscio A. Indirect evaporative cooling by sub-roof forced ventilation to counter extreme heat events. Energy Build 2020;229:110491. https://doi.org/10.1016/j.enbuild.2020.110491.

[25] Chang B, Dang Y, Luo X, Yu CW, Gu Z. Sustainability of evaporative cooling system for environment control for preservation of unearthed historical sites within archaeological museums in china. Sustain 2020;12:1–16. https://doi.org/10.3390/su12239882.

[26] Raza HMU, Ashraf H, Shahzad K, Sultan M, Miyazaki T, Usman M, et al. Investigating applicability of evaporative cooling systems for thermal comfort of poultry birds in Pakistan. Appl Sci 2020;10. https://doi.org/10.3390/app10134445.

[27] Ghoulem M, El Moueddeb K, Nehdi E, Boukhanouf R, Kaiser Calautit J. Greenhouse design and cooling technologies for sustainable food cultivation in hot climates: Review of current practice and future status. Biosyst Eng 2019;183:121–50. https://doi.org/10.1016/j.biosystemseng.2019.04.016.

[28] Porumb B, BĂlan M, Porumb R. Potential of Indirect Evaporative Cooling to Reduce the Energy Consumption in Fresh Air Conditioning Applications. Energy Procedia 2016;85:433–41. https://doi.org/10.1016/j.egypro.2015.12.224.

[29] Chauhan SS, Rajput SPS. Parametric analysis of a combined dew point evaporative-vapour compression based air conditioning system. Alexandria Eng J 2016;55:2333–44. https://doi.org/10.1016/j.aej.2016.05.005.

[30] Chauhan SS, Rajput SPS. Thermodynamic analysis of the evaporative-vapour compression based combined air conditioning system for hot and dry climatic conditions. J Build Eng 2015;4:200–8. https://doi.org/10.1016/j.jobe.2015.09.010.

[31] Dai B, Liu C, Liu S, Wang D, Wang Q, Zou T, et al. Life cycle techno-enviro-economic assessment of dual-temperature evaporation transcritical CO2 high-temperature heat pump systems for industrial waste heat recovery. Appl Therm Eng 2023;219:119570. https://doi.org/10.1016/j.applthermaleng.2022.119570.

[32] Pandelidis D, Anisimov S, Worek WM. Comparison study of the counter-flow regenerative evaporative heat exchangers with numerical methods. Appl Therm Eng 2015;84:211–24. https://doi.org/10.1016/j.applthermaleng.2015.03.058.

[33] Pandelidis D, Anisimov S. Numerical analysis of the selected operational and geometrical aspects of the M-cycle heat and mass exchanger. Energy Build 2015;87:413–24. https://doi.org/10.1016/j.enbuild.2014.11.042.

[34] Anisimov S, Pandelidis D, Jedlikowski A. Performance study of the indirect evaporative air cooler and heat recovery exchanger in air conditioning system during the summer and winter operation. Energy 2015;89:205–25. https://doi.org/10.1016/j.energy.2015.07.070.

[35] Kim M, Kim M, Jeong D, Jeong J. Practical thermal performance correlations for a wet-coil indirect evaporative cooler Practical thermal performance correlations for a wet-coil indirect evaporative cooler. Energy Build 2019;96:285–98. https://doi.org/10.1016/j.enbuild.2015.03.043.

[36] Pandelidis D, Cichoń A, Pacak A, Drąg P, Drąg M, Worek W, et al. Water desalination through the dewpoint evaporative system. Energy Convers Manag 2021;229. https://doi.org/10.1016/j.enconman.2020.113757.

[37] Ranz WE, Marshall WR. Evaporation from drops. 1. Chem Eng Prog 1952:141–6.

[38] Kashyap S, Sarkar J, Kumar A. Performance enhancement of regenerative evaporative cooler by surface alterations and using ternary hybrid nanofluids. Energy 2021;225:120199. https://doi.org/10.1016/j.energy.2021.120199.

[39] Moshari S, Heidarinejad G. Numerical study of regenerative evaporative coolers for sub-wet bulb cooling with cross- and counter-flow configuration. Appl Therm Eng 2015;89:669–83. https://doi.org/10.1016/j.applthermaleng.2015.06.046.

[40] Moshari S, Heidarinejad G, Fathipour A. Numerical investigation of wet-bulb effectiveness and water consumption in one-and two-stage indirect evaporative coolers. Energy Convers Manag 2016;108:309–21. https://doi.org/10.1016/j.enconman.2015.11.022.

[41] Moshari S, Heidarinejad G. Analytical estimation of pressure drop in indirect evaporative coolers for power reduction. Energy Build 2017;150:149–62.

https://doi.org/10.1016/j.enbuild.2017.05.080.

[42] Liu Y, Li JM, Yang X, Zhao X. Two-dimensional numerical study of a heat and mass exchanger for a dew-point evaporative cooler. Energy 2019;168:975–88. https://doi.org/10.1016/j.energy.2018.11.135.

[43] Cui X, Chua KJ, Yang WM. Numerical simulation of a novel energy-efficient dew-point evaporative air cooler. Appl Energy 2014;136:979–88. https://doi.org/10.1016/j.apenergy.2014.04.040.

[44] Kashyap S, Sarkar J, Kumar A. Comparative performance analysis of different novel regenerative evaporative cooling device topologies. Appl Therm Eng 2020;176:115474. https://doi.org/10.1016/j.applthermaleng.2020.115474.

[45] Lin J, Bui DT, Wang R, Chua KJ. On the fundamental heat and mass transfer analysis of the counter-flow dew point evaporative cooler. Appl Energy 2018;217:126–42. https://doi.org/10.1016/j.apenergy.2018.02.120.

[46] Wan Y, Soh A, Shao Y, Cui X, Tang Y, Chua KJ. Numerical study and correlations for heat and mass transfer coefficients in indirect evaporative coolers with condensation based on orthogonal test and CFD approach. Int J Heat Mass Transf 2020;153:119580. https://doi.org/10.1016/j.ijheatmasstransfer.2020.119580.

[47] Dowdy JA, Reid RL, Handy ET. Experimental determination of heat- and mass-transfer coefficients in aspen pads (Conference)|OSTI.GOV 1986. https://www.osti.gov/biblio/6844472-experimental-determination-heat-mass-transfer-coefficients-aspen-pads (accessed June 7, 2021).

[48] Awad MM. Heat Transfer for Laminar Thermally Developing Flow in Parallel-Plates Using the Asymptotic Method. Therm. Issues Emerg. Technol. ThETA 3, Cairo, Egypt,: IEEE; 2010, p. 371–87.

[49] Baakeem SS, Orfi J, Bessadok-Jemai A. Thermodynamic and economic analysis of the performance of a direct evaporative cooler working under extreme summer weather conditions. J Mech Sci Technol 2018;32:1815–25. https://doi.org/10.1007/s12206-018-0338-y.

[50] Heidarinejad G, Moshari S. Novel modeling of an indirect evaporative cooling system with cross-flow configuration. Energy Build 2015;92:351–62. https://doi.org/10.1016/j.enbuild.2015.01.034.

[51] Lin J, Wang RZ, Kumja M, Bui TD, Chua KJ. Modelling and experimental investigation of the cross-flow dew point evaporative cooler with and without dehumidification. Appl Therm Eng 2017;121:1–13. https://doi.org/10.1016/j.applthermaleng.2017.04.047.

[52] Lin J, Thu K, Bui TD, Wang RZ, Ng KC, Chua KJ. Study on dew point evaporative cooling system with counter-flow configuration. Energy Convers Manag 2016;109:153–65. https://doi.org/10.1016/j.enconman.2015.11.059.

[53] Chen Y, Yang H, Luo Y. Parameter sensitivity analysis and configuration optimization of indirect evaporative cooler (IEC) considering condensation. Appl Energy 2017;194:440–53. https://doi.org/10.1016/j.apenergy.2016.06.121.

[54] Aljubury IMA, Ridha HD a. Enhancement of evaporative cooling system in a greenhouse using geothermal energy. Renew Energy 2017;111:321–31. https://doi.org/10.1016/j.renene.2017.03.080.

[55] Buker MS, Mempouo B, Riffat SB. Experimental investigation of a building integrated photovoltaic/thermal roof collector combined with a liquid desiccant enhanced indirect evaporative cooling system. Energy Convers Manag 2015;101:239–54. https://doi.org/10.1016/j.enconman.2015.05.026.

[56] Khalajzadeh V, Farmahini-Farahani M, Heidarinejad G. A novel integrated system of ground heat exchanger and indirect evaporative cooler. Energy Build 2012;49:604–10. https://doi.org/10.1016/j.enbuild.2012.03.009.

[57] Heidarinejad G, Khalajzadeh V, Delfani S. Performance analysis of a ground-assisted direct evaporative cooling air conditioner. Build Environ 2010;45:2421–9. https://doi.org/10.1016/j.buildenv.2010.05.009.

[58] Zhan C, Duan Z, Zhao X, Smith S, Jin H, Riffat S. Comparative study of the performance of the M-cycle counter-flow and cross-flow heat exchangers for indirect evaporative cooling - Paving the path toward sustainable cooling of buildings. Energy 2011;36:6790–805. https://doi.org/10.1016/j.energy.2011.10.019.

[59] Duan Z, Zhao X, Li J. Design, fabrication and performance evaluation of a compact regenerative evaporative cooler: Towards low energy cooling for buildings. Energy 2017;140:506–19. https://doi.org/10.1016/j.energy.2017.08.110.

[60] Zhan C, Zhao X, Smith S, Riffat SB. Numerical study of a M-cycle cross-flow heat exchanger for indirect evaporative cooling. Build Environ 2011;46:657–68. https://doi.org/10.1016/j.buildenv.2010.09.011.

[61] Zhao X, Li JM, Riffat SB. Numerical study of a novel counter-flow heat and mass exchanger for dew point evaporative cooling. Appl Therm Eng 2008;28:1942–51. https://doi.org/10.1016/j.applthermaleng.2007.12.006.

[62] Zheng B, Guo C, Chen T, Shi Q, Lv J, You Y. Development of an experimental validated model of cross-flow indirect evaporative cooler with condensation. Appl Energy 2019;252:113438. https://doi.org/10.1016/j.apenergy.2019.113438.

[63] Xu P, Ma X, Diallo TMO, Zhao X, Fancey K, Li D, et al. Numerical investigation of the energy performance of a guideless irregular heat and mass exchanger with corrugated heat transfer surface for dew point cooling. Energy 2016;109:803–17. https://doi.org/10.1016/j.energy.2016.05.062.

[64] Guo C, Liu Q, Zheng B, You Y, Li Y. Development of model based on condensation area ratio and effect on heat transfer capacity of indirect evaporative cooling. Appl Therm Eng 2020;164:114557. https://doi.org/10.1016/j.applthermaleng.2019.114557.

[65] Li WY, Li YC, Zeng L yue, Lu J. Comparative study of vertical and horizontal indirect evaporative cooling heat recovery exchangers. Int J Heat Mass Transf 2018;124:1245–61. https://doi.org/10.1016/j.ijheatmasstransfer.2018.04.041.

[66] Wang Y, Huang X, Li L. Comparative study of the cross-flow heat and mass exchangers for indirect evaporative cooling using numerical methods. Energies 2018;11. https://doi.org/10.3390/en11123374.

[67] Yutong L, Hongxing Y. Investigation on solar desiccant dehumidification process for energy conservation of central air-conditioning systems. Appl Therm Eng 2008;28:1118–26. https://doi.org/10.1016/j.applthermaleng.2007.08.006.

[68] Chen Y, Yang H, Luo Y. Investigation on solar assisted liquid desiccant dehumidifier

709 and evaporative cooling system for fresh air treatment. Energy 2018;143:114–27.
710 https://doi.org/10.1016/j.energy.2017.10.124.

711 [69] Yang H, Shi W, Chen Y, Min Y. Research development of indirect evaporative cooling
712 technology: An updated review. Renew Sustain Energy Rev 2021;145:111082.
713 https://doi.org/10.1016/j.rser.2021.111082.

714 [70] Boukhanouf R, Alharbi A, Ibrahim HG, Amer O, Worall M. Computer modelling and
715 experimental investigation of building integrated sub-wet bulb temperature evaporative
716 cooling system. Appl Therm Eng 2017;115:201–11.
717 https://doi.org/10.1016/j.applthermaleng.2016.12.119.

718 [71] Rogdakis ED, Koronaki IP, Tertipis DN. Experimental and computational evaluation of
719 a Maisotsenko evaporative cooler at Greek climate. Energy Build 2014;70:497–506.
720 https://doi.org/10.1016/j.enbuild.2013.10.013.

721 [72] De Antonellis S, Joppolo CM, Leone C, Liberati P, Milani S. Indirect evaporative
722 cooling systems: An experimental analysis in summer condition. Energy Procedia
723 2017;140:467–74. https://doi.org/10.1016/j.egypro.2017.11.158.

724 [73] Xiao N, Zhang Q, Ligrani PM, Mongia R. Thermal performance of dimpled surfaces in
725 laminar flows. Int J Heat Mass Transf 2009;52:2009–17.
726 https://doi.org/10.1016/j.ijheatmasstransfer.2008.11.006.

727 [74] Kumar P, Kumar A, Chamoli S, Kumar M. Experimental investigation of heat transfer
728 enhancement and fluid flow characteristics in a protruded surface heat exchanger tube.
729 Exp Therm Fluid Sci 2016;71:42–51.
730 https://doi.org/10.1016/j.expthermflusci.2015.10.014.

731 [75] Liberati P, De Antonellis S, Leone C, Joppolo CM, Bawa Y. Indirect Evaporative
732 cooling systems: Modelling and performance analysis. Energy Procedia 2017;140:475–
733 85. https://doi.org/10.1016/j.egypro.2017.11.159.

734 [76] De Antonellis S, Joppolo CM, Liberati P, Milani S, Romano F. Modeling and
735 experimental study of an indirect evaporative cooler. Energy Build 2017;142:147–57.
736 https://doi.org/10.1016/j.enbuild.2017.02.057.

737 [77] Lee J, Choi B, Lee DY. Comparison of configurations for a compact regenerative
738 evaporative cooler. Int J Heat Mass Transf 2013;65:192–8.
739 https://doi.org/10.1016/j.ijheatmasstransfer.2013.05.068.

740 [78] Kashyap S, Sarkar J, Kumar A. Effect of surface modifications and using hybrid
741 nanofluids on energy-exergy performance of regenerative evaporative cooler. Build
742 Environ 2021;189:107507. https://doi.org/10.1016/j.buildenv.2020.107507.

743 [79] Zhang Y, Jiang C, Yang Z, Zhang Y, Bai B. Numerical study on heat transfer
744 enhancement in capsule-type plate heat exchangers. Appl Therm Eng 2016;108:1237–
745 42. https://doi.org/10.1016/j.applthermaleng.2016.08.033.

746 [80] Kabeel AE, Abdelgaied M. Numerical and experimental investigation of a novel
747 configuration of indirect evaporative cooler with internal baffles. Energy Convers
748 Manag 2016;126:526–36. https://doi.org/10.1016/j.enconman.2016.08.028.

749 [81] Kabeel AE, Bassuoni MM, Abdelgaied M. Experimental study of a novel integrated
750 system of indirect evaporative cooler with internal baffles and evaporative condenser.
751 Energy Convers Manag 2017;138:518–25.

https://doi.org/10.1016/j.enconman.2017.02.025.

[82] Riangvilaikul B, Kumar S. Numerical study of a novel dew point evaporative cooling system. Energy Build 2010;42:2241–50. https://doi.org/10.1016/j.enbuild.2010.07.020.

[83] Min Y, Chen Y, Yang H, Guo C. Characteristics of primary air condensation in indirect evaporative cooler : Theoretical analysis and visualized validation. Build Environ 2020;174:106783.

[84] Hasan A. Indirect evaporative cooling of air to a sub-wet bulb temperature. Appl Therm Eng 2010;30:2460–8. https://doi.org/10.1016/j.applthermaleng.2010.06.017.

[85] Jradi M, Riffat S. Experimental and numerical investigation of a dew-point cooling system for thermal comfort in buildings. Appl Energy 2014;132:524–35. https://doi.org/10.1016/J.APENERGY.2014.07.040.

[86] Anisimov S, Pandelidis D, Danielewicz J. Numerical analysis of selected evaporative exchangers with the Maisotsenko cycle. Energy Convers Manag 2014;88:426–41. https://doi.org/10.1016/j.enconman.2014.08.055.

[87] Lin J, Thu K, Bui TD, Wang RZ, Ng KC, Kumja M, et al. Unsteady-state analysis of a counter-flow dew point evaporative cooling system. Energy 2016;113:172–85. https://doi.org/10.1016/j.energy.2016.07.036.

[88] El-Dessouky H, Ettouney H, Al-Zeefari A. Performance analysis of two-stage evaporative coolers. Chem Eng J 2004;102:255–66. https://doi.org/10.1016/j.cej.2004.01.036.

[89] Kim MH, Kim JH, Choi AS, Jeong JW. Experimental study on the heat exchange effectiveness of a dry coil indirect evaporation cooler under various operating conditions. Energy 2011;36:6479–89. https://doi.org/10.1016/j.energy.2011.09.018.

[90] Martín RH. Numerical simulation of a semi-indirect evaporative cooler. Energy Build 2009;41:1205–14. https://doi.org/10.1016/j.enbuild.2009.06.008.

[91] Jamil MA, Zubair SM. Design and analysis of a forward feed multi-effect mechanical vapor compression desalination system: An exergo-economic approach. Energy 2017;140:1107–20. https://doi.org/https://doi.org/10.1016/j.energy.2017.08.053.

[92] Jamil MA, Zubair SM. On thermoeconomic analysis of a single-effect mechanical vapor compression desalination system. Desalination 2017;420:292–307.

Appendix A: Heat transfer coefficient trends from earlier studies.

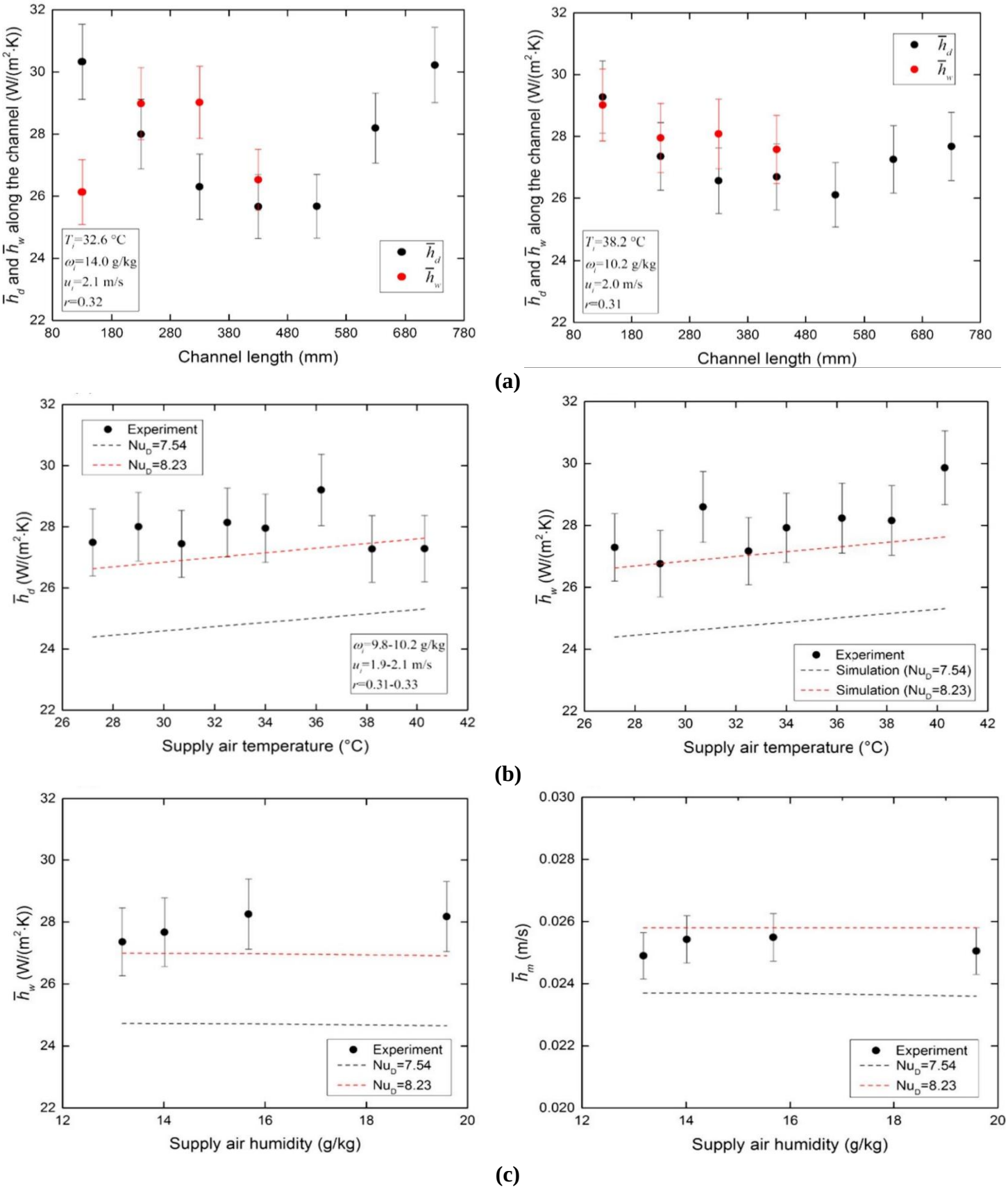

Figure A-1 Effect of parameters on heat transfer coefficient (a) channel length, (b) supply air temperature, (c) supply air humidity Lin et al. [45] .

787 Heat transfer coefficient characteristics studied by Wan et al. [46].

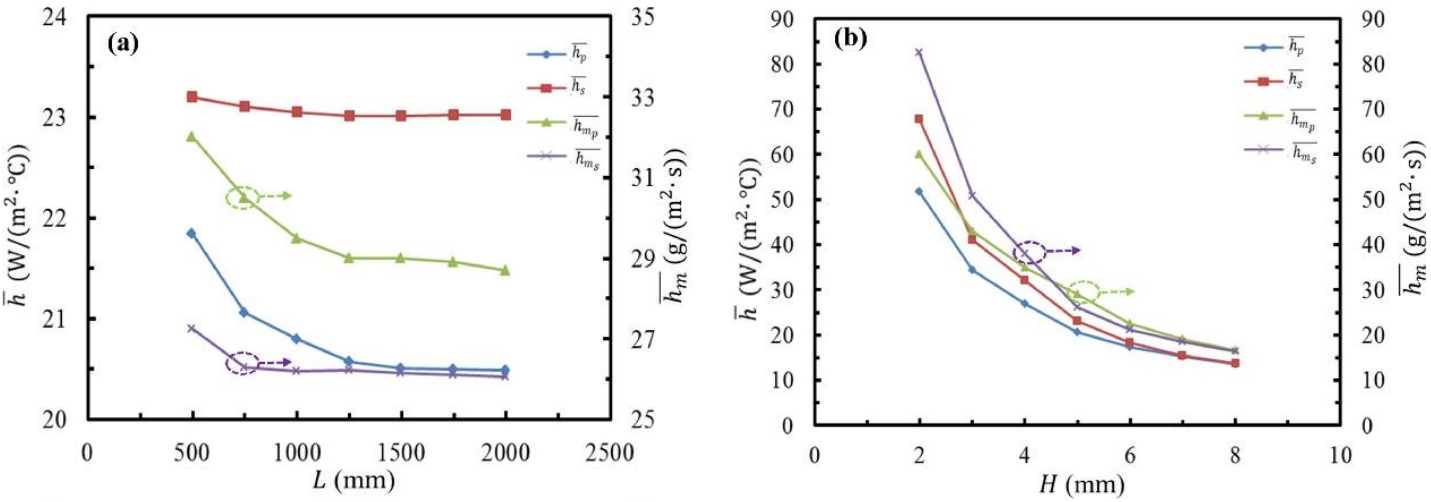

788 Figure A-2. Heat transfer coefficients against channel length (L) and gap (H) [46].

789

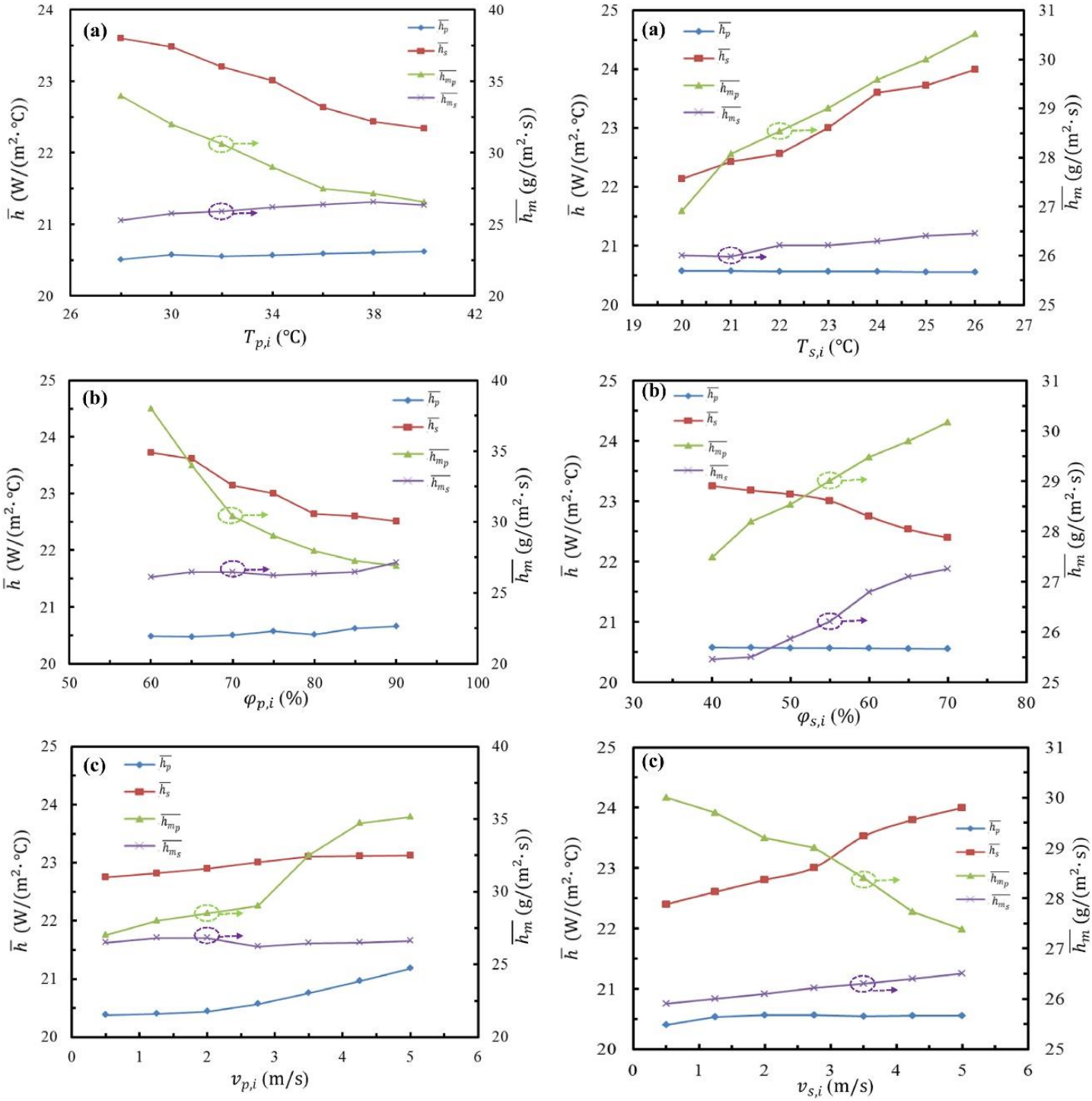

790 Figure A-3. Heat transfer coefficient vs outdoor (primary) and working (secondary) air
791 characteristics [46].

792

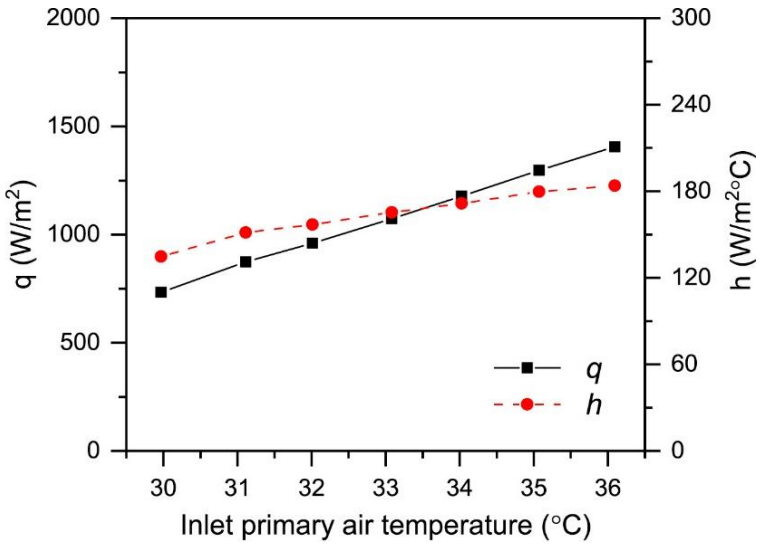

Figure A-4. Heat transfer coefficient under condensation conditions in dry channel [83].